Research Paper

Evaluation of ^{111}In-Labeled Cyclic RGD Peptides: Effects of Peptide and Linker Multiplicity on Their Tumor Uptake, Excretion Kinetics and Metabolic Stability

Jiyun Shi[1,2], Yang Zhou[1], Sudipta Chakraborty[1], Young-Seung Kim[1], Bing Jia[2], Fan Wang[2] and Shuang Liu[1✉]

1. School of Health Sciences, Purdue University, IN 47907, USA
2. Medical Isotopes Research Center, Peking University, Beijing 100083, China

✉ Corresponding author: School of Health Sciences, Purdue University, 550 Stadium Mall Drive, West Lafayette, IN 47907. Phone: 765-494-0236; Fax 765-496-1377; Email: liu100@purdue.edu

Abstract

Purpose: The purpose of this study was to demonstrate the valence of cyclic RGD peptides, P-RGD (PEG$_4$-c(RGDfK): PEG$_4$ = 15-amino-4,710,13-tetraoxapentadecanoic acid), P-RGD$_2$ (PEG$_4$-E[c(RGDfK)]$_2$, 2P-RGD$_4$ (E{PEG$_4$-E[c(RGDfK)]$_2$}$_2$, 2P4G-RGD$_4$ (E{PEG$_4$-E[G$_3$-c(RGDfK)]$_2$}$_2$: G$_3$ = Gly-Gly-Gly) and 6P-RGD$_4$ (E{PEG$_4$-E[PEG$_4$-c(RGDfK)]$_2$}$_2$) in binding to integrin $\alpha_v\beta_3$, and to assess the impact of peptide and linker multiplicity on biodistribution properties, excretion kinetics and metabolic stability of their corresponding ^{111}In radiotracers.

Methods: Five new RGD peptide conjugates (DOTA-P-RGD (DOTA =1,4,7,10-tetraazacyclododecane-1,4,7,10-tetracetic acid), DOTA-P-RGD$_2$, DOTA-2P-RGD$_4$, DOTA-2P4G-RGD$_4$, DOTA-6P-RGD$_4$), and their ^{111}In complexes were prepared. The integrin $\alpha_v\beta_3$ binding affinity of cyclic RGD conjugates were determined by a competitive displacement assay against ^{125}I-c(RGDyK) bound to U87MG human glioma cells. Biodistribution, planar imaging and metabolism studies were performed in athymic nude mice bearing U87MG human glioma xenografts.

Results: The integrin $\alpha_v\beta_3$ binding affinity of RGD conjugates follows the order of: DOTA-6P-RGD$_4$ (IC$_{50}$ = 0.3 ± 0.1 nM) ~ DOTA-2P4G-RGD$_4$ (IC$_{50}$ = 0.2 ± 0.1 nM) ~ DOTA-2P-RGD$_4$ (IC$_{50}$ = 0.5 ± 0.1 nM) > DOTA-3P-RGD$_2$ (DOTA-PEG$_4$-E[PEG$_4$-c(RGDfK)]$_2$: IC$_{50}$ = 1.5 ± 0.2 nM) **>** DOTA-P-RGD$_2$ (IC$_{50}$ = 5.0 ± 1.0 nM) >> DOTA-P-RGD (IC$_{50}$ = 44.3 ± 3.5 nM) ~ c(RGDfK) (IC$_{50}$ = 49.9 ± 5.5 nM) >> DOTA-6P-RGK$_4$ (IC$_{50}$ = 437 ± 35 nM). The fact that DOTA-6P-RGK$_4$ had much lower integrin $\alpha_v\beta_3$ binding affinity than DOTA-6P-RGD$_4$ suggests that the binding of DOTA-6P-RGD$_4$ to integrin $\alpha_v\beta_3$ is RGD-specific. This conclusion is consistent with the lower tumor uptake for [111]In(DOTA-6P-RGK$_4$) than that for [111]In(DOTA-6P-RGD$_4$). It was also found that the G$_3$ and PEG$_4$ linkers between RGD motifs have a significant impact on the integrin $\alpha_v\beta_3$-targeting capability, biodistribution characteristics, excretion kinetics and metabolic stability of ^{111}In-labeled cyclic RGD peptides.

Conclusion: On the basis of their integrin $\alpha_v\beta_3$ binding affinity and tumor uptake of their corresponding ^{111}In radiotracers, it was conclude that 2P-RGD$_4$, 2P4G-RGD$_4$ and 6P-RGD$_4$ are most likely bivalent in binding to integrin $\alpha_v\beta_3$, and extra RGD motifs might contribute to the long tumor retention times of [111]In(DOTA-2P-RGD$_4$), [111]In(DOTA-2P4G-RGD$_4$) and [111]In(DOTA-6P-RGD$_4$) than that of [111]In(DOTA-3P-RGD$_3$) at 72 h p.i. Among the ^{111}In-labeled cyclic RGD tetramers evaluated in the glioma model, [111]In(DOTA-2P4G-RGD$_4$) has very high tumor uptake with the best tumor/kidney and tumor/liver ratios, suggesting that [90]Y(DOTA-2P4G-RGD$_4$) and

^{177}Lu(DOTA-2P4G-RGD$_4$) might have the potential for targeted radiotherapy of integrin $\alpha_v\beta_3$-positive tumors.

Introduction

Over last several years, many multimeric cyclic RGD peptides, such as E[c(RGDfK)]$_2$ (RGD$_2$) and E{E[c(RGDfK)]$_2$}$_2$ (RGD$_4$), have been used to develop the integrin $\alpha_v\beta_3$-targeted radiotracers for noninvasive imaging of rapidly growing and metastatic tumors [1-14]. Multiple cyclic RGD moieties are utilized to maximize their integrin $\alpha_v\beta_3$ binding affinity and the radiotracer tumor uptake [9, 15-46]. It was found that the radiolabeled (^{99m}Tc, ^{18}F, ^{64}Cu, ^{68}Ga and ^{111}In) cyclic RGD tetramers have better tumor-targeting capability as evidenced by their higher tumor uptake with longer tumor retention time than their corresponding dimeric and monomeric counterparts [20, 22, 29, 32, 34, 35, 44, 46]. It was also found that cyclic RGD tetramers, such as DOTA-RGD$_4$ (DOTA = 1,4,7,10-tetraazacyclodo-decane-1,4,7,10-tetracetic acid) and DOTA-E{G$_3$-E[G$_3$-c(RGDfK)]$_2$}$_2$ (Figure 1: DOTA-6G-RGD$_2$) are likely bivalent in binding to integrin $\alpha_v\beta_3$ even though they contain four identical RGD motifs [46]. The key for bivalency is the distance between two RGD motifs [36-38]. For example, RGD$_2$ was monovalent whereas PEG$_4$-E[PEG$_4$-c(RGDfK)]$_2$ (3P-RGD$_2$: PEG$_4$ = 15-amino-4,7,10,13-tetraoxapentadecanoic acid) and G$_3$-E[G$_3$-c(RGDfK)]$_2$ (3G-RGD$_2$: G$_3$ = Gly-Gly-Gly) are bivalent because of the increased distance between two cyclic RGD motifs for simultaneous integrin $\alpha_v\beta_3$ binding [38, 45].

To further prove the "bivalency concept", we prepared three new cyclic RGD peptide tetramers (Figure 1: 2P-RGD$_4$, 2P4G-RGD$_4$ and 6P-RGD$_4$). We were particularly interested in these three peptides because they contain different number of G$_3$ and PEG$_4$ linkers between cyclic RGD motifs. The main objective of this study was to demonstrate their valence in binding to integrin $\alpha_v\beta_3$, and to assess the impact of cyclic RGD peptide and linker multiplicity on biodistribution properties, excretion kinetics and metabolic stability of ^{111}In radiotracers. In this report, we present the synthesis and biological evaluation of RGD tetramer conjugates, DOTA-2P-RGD$_4$, DOTA-2P4G-RGD$_4$ and DOTA-6P-RGD$_4$, and their ^{111}In complexes. A whole-cell competitive displacement assay was used to determine their integrin $\alpha_v\beta_3$ binding affinities against ^{125}I-c(RGDyK) bound to U87MG human glioma cells. Biodistribution and planar imaging studies performed in the athymic nude mice bearing U87MG glioma xenografts. For comparison purposes, we prepared and evaluated conjugates DOTA-PEG$_4$-c(RGDfK) (DOTA-P-RGD), DOTA-PEG$_4$-E[c(RGDfK)]$_2$ (DOTA-P-RGD$_2$), and their ^{111}In radiotracers using the same in vitro and in vivo assays. In addition, we prepared a "scrambled" peptide conjugate DOTA-E{PEG$_4$-E[PEG$_4$-c(RGKfD)]$_2$}$_2$ (DOTA-6P-RGK$_4$), which has the same amino acid residues as those in DOTA-6P-RGD$_4$ using c(RGKfD) motifs instead of c(RGDfK), and ^{111}In(DOTA-6P-RGK$_4$) to demonstrate the RGD-specificity of ^{111}In radiotracers.

Materials and Methods

Materials and Instruments. Chemicals were purchased from *Sigma/Aldrich* (St. Louis, MO), and were used without purification. Cyclic peptides, PEG$_4$-c(RGDfK) (P-RGD), PEG$_4$-E[G$_3$-c(RGDfK)]$_2$ (P2G-RGD$_2$), PEG$_4$-E[PEG$_4$-c(RGDfK)]$_2$ (3P-RGD$_2$) and PEG$_4$-E[PEG$_4$-c(RGKfD)]$_2$ (3P-RGK$_2$), were all custom-made by the Peptides International, Inc. (Louisville, KY). DOTA-OSu (1,4,7,10-tetraazacyclodo-decane-4,7,10-triacetic acid-1-acetate(N-hydroxysucci-namide)) was purchased from Macrocyclics (Dallas, TX). The Boc-protected glutamic acid N-hydroxysuccinamide ester (Boc-E(OSu)$_2$) and PEG$_4$-E[c(RGDfK)]$_2$ (P-RGD$_2$) were prepared according to the methods described in our previous reports [23-26]. Syntheses and biological evaluations of DOTA-3P-RGD$_2$ and ^{111}In(DOTA-3P-RGD$_2$) were reported in our previous communication [45]. ESI (electron-spray ionization) mass spectral data were obtained in positive mode using a Finnigan LCQ classic mass spectrometer, School of Pharmacy, Purdue University. The MALDI (matrix assisted laser desorption ionizations) mass spectral data were collected using an Applied Biosystems Voyager DE PRO mass spectrometer (Framingham, MA), the Department of Chemistry, Purdue University. ^{111}InCl$_3$ was obtained from Perkin-Elmer Life Sciences (North Billerica, MA). The NH$_4$OAc buffer for ^{111}In-labeling studies was passed over a Chelex-100 column (1×15 cm) to minimize the trace metal contaminants.

HPLC Methods. The HPLC method (Method 1) used a LabAlliance HPLC system equipped with a UV/vis detector (λ=254 nm) and Zorbax C$_{18}$ semi-prep column (9.4 mm x 250 mm, 100 Å pore size; Agilent Technologies, Santa Clara, CA). The flow rate was 2.5 mL/min with the gradient mobile phase going

from 90% A (0.1% TFA in water) and 10% (0.1% TFA in acetonitrile) at 0 min to 20% B at 5 min and to 40% B at 20 min. The radio-HPLC method (Method 2) used the LabAlliance HPLC system equipped with a β-ram IN/US detector (Tampa, FL) and Zorbax C_{18} column (4.6 mm x 250 mm, 300 Å pore size; Agilent Technol-

ogies, Santa Clara, CA). The flow rate was 1 mL/min. The mobile phase was isocratic with 90% A (25 mM NH_4OAc, pH = 6.8) and 10% B (acetonitrile) at 0 – 5 min, followed by a gradient mobile phase going from 10% B at 5 min to 20% B at 15 min and to 50% B at 20 min.
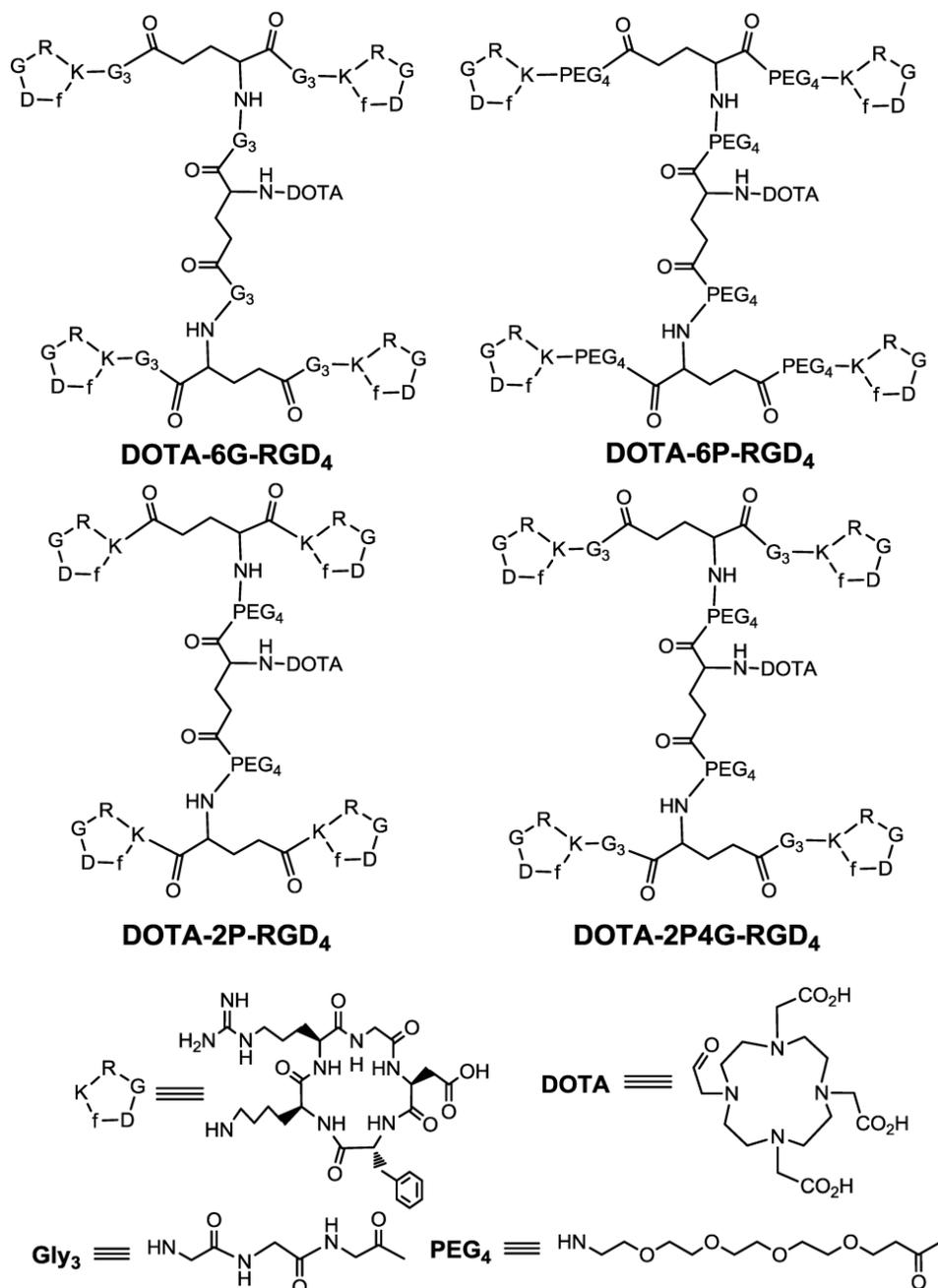
Figure 1. Cyclic RGD peptide tetramer conjugates: DOTA-6G-RGD$_4$, DOTA-6P-RGD$_4$, DOTA-2P-RGD$_4$ and DOTA-2P4G-RGD$_4$.

DOTA-PEG₄-c(RGDfK)   (DOTA-P-RGD). PEG$_4$-c(RGDfK) (7.1 mg, ~8.3 μmol) and DOTA-OSu (5.5 mg, ~11.0 μmol) were dissolved in 1 mL of

anhydrous dimethylformamide (DMF). The pH value in the reaction mixture was adjusted to 8.5 – 9.0 using diisopropylethylamine (DIEA). The mixture was then

stirred overnight at room temperature. After addition of 3 mL of 100 mM NH_4OAc buffer (pH = 7.0), the resulting solution was subjected to HPLC-purification (Method 1). The fraction at ~ 12.5 min was collected. Lyophilization of collected fractions afforded conjugate DOTA-P-RGD. The yield was 4.1 mg (~40%). ESI-MS (positive mode): m/z =1237.58 for $[M + H]^+$ (M =1236.6 calcd. for $C_{54}H_{88}N_{14}O_{19}$).

DOTA-PEG$_4$-[c(RGDfK)]$_2$ (DOTA-P-RGD$_2$). PEG$_4$-[c(RGDfK)]$_2$ (1.8 mg, 1.1 µmol) and DOTA-OSu (2.1 mg, 4.2 µmol) were dissolved in DMF (1 mL). The pH in the reaction mixture was adjusted to 8.5 – 9.0 using DIEA. The mixture was stirred for 2 h at room temperature. Upon addition of 2 mL NH_4OAc buffer (100 mM, pH = 7.0), the product was separated by HPLC (Method 1). Lyophilization of the collected fractions at ~ 16.4 min afforded 0.9 mg of DOTA-P-RGD$_2$ (~41%) with 95% HPLC purity. The yield was ESI-MS (positive mode) for m/z = 1951.5 for $[M + H]^+$, 976.6 for $[M + 2H]^{2+}$ and 1974.4 for $[M + Na]^+$ (M = 1950.2 calcd. for $[C_{86}H_{134}N_{24}O_{28}]^+$).

Boc-E{PEG$_4$-E[c(RGDfK)]$_2$}$_2$ (Boc-2P-RGD$_4$). To a solution of Boc-E(OSu)$_2$ (1.1 mg, 2.5 µmol) in 1 mL of DMF were added PEG$_4$-[c(RGDfK)]$_2$ (5.8 mg, 3.4 µmol) and DIEA (2 drops). The reaction mixture was stirred for 2 h at room temperature. The reaction was terminated by adding 3 mL NH_4OAc buffer (100 mM, pH = 7.0). The product was isolated by HPLC (Method 1). Lyophilization of collected fractions at 18.2 min afforded Boc-2P-RGD$_4$. The yield was 4.5 mg (~79%). ESI-MS (positive mode): m/z = 3344.2 for $[M + H]^+$ and 1671.9 for $[M + 2H]^{2+}$ (M = 3342.7 calcd. for $[C_{150}H_{229}N_{41}O_{46}]^+$).

E{PEG$_4$-E[c(RGDfK)]$_2$}$_2$ (2P-RGD$_4$). The Boc-2P-RGD$_4$ (4.3 mg, 1.3 µmol) was dissolved in 2 mL of TFA. After standing at room temperature for 5 min, TFA was removed. The residue was dissolved in 2 mL of 0.1 M NH_4OAc buffer (100 mM, pH = 7.0). The product was separated by HPLC (Method 1). Lyophilization of collected fractions at 15.7 min afforded 2P-RGD$_4$. The yield was 2.6 mg (~59%). ESI-MS (positive mode): m/z = 3244.0 for $[M + H]^+$ and 1620.5 for $[M + 2H]^{2+}$ (M = 3242.6 calcd. for $[C_{145}H_{221}N_{41}O_{44}]^+$).

DOTA-E{PEG$_4$-E[c(RGDfK)]$_2$}$_2$ (DOTA-2P-RGD$_4$). DOTA-OSu (3.3 mg, 6.5 µmol) and 2P-RGD$_4$ (2.2 mg, 0.7 µmol) were dissolved in 1 mL of anhydrous DMF. After addition of DIEA (3 drops), the reaction mixture was stirred for 2 h at room temperature. Upon addition of 2 mL NH_4OAc buffer (100 mM, pH = 7.0), the product was isolated by HPLC (Method 1). Lyophilization of collected fraction at 16.1 min afforded conjugate DOTA-2P-RGD$_4$ with >95% HPLC purity. The yield was 1.4 mg (~56%). MALDI-MS: m/z = 3626.4 for $[M + H]^+$ (M = 3626.8 calcd. for

$[C_{161}H_{247}N_{45}O_{51}]^+$).

Boc-E{PEG$_4$-E[Gly$_3$-c(RGDfK)]$_2$}$_2$ (Boc-2P4G-RGD$_4$). To a solution of Boc-E(OSu)$_2$ (3.8 mg, 8.6 µmol) in DMF (3 mL) were added P2G-RGD$_2$ (20.9 mg, 11.0 µmol) and excess DIEA (3 drops). The mixture was stirred for 3 h at room temperature. The reaction was terminated by addition of 3 mL NH_4OAc buffer (100 mM, pH = 7.0). The product was isolated by HPLC (Method 1). Lyophilization of collected fractions at 16.3 min afforded Boc-2P4G-RGD$_4$. The yield was 9.5 mg (~ 43 %). ESI-MS (positive mode): m/z = 4028.0 for $[M + H]^+$ (M = 4027.3 calcd. for $[C_{174}H_{265}N_{53}O_{58}]^+$).

E{PEG$_4$-E[Gly$_3$-c(RGDfK)]$_2$}$_2$ (2P4G-RGD$_4$). The Boc-protected 2P4G-RGD$_4$ (9.0 mg, 2.2 µmol) was dissolved in 2 mL of TFA. After standing at room temperature for 5 min, TFA was removed, and the residue was dissolved in 2 mL of 0.1 M NH_4OAc buffer (100 mM, pH = 7.0). The product was separated from the mixture by HPLC (Method 1). Lyophilization of collected fractions at 14.2 min afforded 2P4G-RGD$_4$. The yield was 4.0 mg (~46%). ESI-MS (positive mode): m/z = 3927.9 for $[M + H]^+$ and 1964.6 for $[M + 2H]^{2+}$ (M = 3927.3 calcd. for $[C_{169}H_{257}N_{53}O_{56}]^+$).

DOTA-E{PEG$_4$-E[Gly$_3$-c(RGDfK)]$_2$}$_2$ (DOTA-2P4G-RGD$_4$). DOTA-OSu (5.8 mg, 11.5 µmol) and 2P4G-RGD$_4$ (3.2 mg, 0.8 µmol) were dissolved in DMF (2 mL). After addition of DIEA (2 drops), the mixture was stirred for 2 h at room temperature. Upon addition of 2 mL NH_4OAc buffer (100 mM, pH = 7.0), the product was separated by HPLC (Method 1). Lyophilization of collected fraction at 14.9 min afforded conjugate DOTA-2P4G-RGD$_4$ with >95% HPLC purity. The yield was 2.2 mg (~64%). MALDI-MS: m/z = 4315.4 for $[M + H]^+$ (M = 4313.6 calcd. for $[C_{185}H_{283}N_{57}O_{63}]^+$).

Boc-E{PEG$_4$-E[PEG$_4$-c(RGDfK)]$_2$}$_2$ (Boc-6P-RGD$_4$). To a solution of Boc-E(OSu)$_2$ (2.1 mg, 4.75 µmol) in DMF (2 mL) was added 3P-RGD$_2$ (22 mg, 10.7 µmol). After addition of excess DIEA, the reaction mixture was stirred for 3 h at room temperature. The reaction was terminated by addition of 3 mL NH_4OAc buffer (100 mM, pH = 7.0). The product was separated by HPLC (Method 1). Lyophilization of collected fractions at 18.5 min afforded desired product Boc-6P-RGD$_4$. The yield was 15.6 mg (~76%). MALDI-MS: m/z = 4333.8 for $[M + H]^+$ (M = 4331.8 calcd. for $[C_{194}H_{313}N_{45}O_{66}]^+$).

E{PEG$_4$-E[PEG$_4$-c(RGDfK)]$_2$}$_2$ (6P-RGD$_4$). The Boc-protected 6P-RGD$_4$ (15.6 mg, 3.6 µmol) was dissolved in 2 mL of TFA. After standing 5 min at room temperature, TFA was removed, and the residue was dissolved in 2 mL of NH_4OAc buffer (100 mM, pH = 7.0). The product was separated from the mixture by

HPLC (Method 1). Lyophilization of collected fractions at 17.3 min afforded the desired product 6P-RGD$_4$. The yield was 14.0 mg (~92%). MALDI-MS: m/z = 4233.4 for $[M + H]^+$ (M = 4231.7 calcd. for $[C_{189}H_{305}N_{45}O_{64}]^+$).

DOTA-E{PEG$_4$-E[PEG$_4$-c(RGDfK)]$_2$}$_2$ (DOTA-6P-RGD$_4$). DOTA-OSu (7.7 mg, 15.3 μmol) and 6P-RGD$_4$ (3.8 mg, 0.9 μmol) were dissolved in 1 mL of anhydrous DMF. After addition of DIEA (3 drops), the reaction mixture was stirred for 2 h at room temperature. Upon addition of 2 mL NH$_4$OAc buffer (100 mM, pH = 7.0), the product was separated from the mixture by HPLC (Method 1). Lyophilization of collected fraction at 18.2 min afforded DOTA-6P-RGD$_4$ with >95% purity. The yield was 1.8 mg (~43%). MALDI-MS: m/z = 4622.7 for $[M + H]^+$ (M = 4618.1 calcd. for $[C_{205}H_{331}N_{49}O_{71}]^+$).

Boc-E{PEG$_4$-E[PEG$_4$-c(RGKfD)]$_2$}$_2$ (Boc-6P-RGK$_4$). To a solution of the Boc-E(OSu)$_2$ (5.5 mg, 12.5 μmol) in DMF (2 mL) was added 3P-RGK$_2$ (30 mg, 14.6 μmol). After addition of excess DIEA, the reaction mixture was stirred for 3 h at room temperature. The reaction was terminated by addition of 3 mL NH$_4$OAc buffer (100 mM, pH = 7.0). The product was isolated by HPLC (Method 1). Lyophilization of collected fractions at 18.5 min afforded desired product Boc-6P-RGK$_4$. The yield was 15.6 mg (~49%). MALDI-MS: m/z = 4334.9 for $[M + H]^+$ (M = 4331.8 calcd. for $[C_{194}H_{313}N_{45}O_{66}]^+$).

E{PEG$_4$-E[PEG$_4$-c(RGKfD)]$_2$}$_2$ (6P-RGK$_4$). Boc-6P-RGK$_4$ (15.5 mg, 3.6 μmol) was dissolved in TFA (2 mL). After 5 min at room temperature, TFA was removed, and the residue was dissolved in 2 mL of NH$_4$OAc buffer (100 mM, pH = 7.0). The product was separated from the mixture by HPLC (Method 1). Lyophilization of collected fractions at 15.8 min afforded 6P-RGK$_4$. The yield was 14.0 mg (~93%). MALDI-MS: m/z = 4233.4 for $[M + H]^+$ (M = 4231.7 calcd. for $[C_{189}H_{305}N_{45}O_{64}]^+$).

DOTA-E{PEG$_4$-E[PEG$_4$-c(RGKfD)]$_2$}$_2$ (DOTA-6P-RGK$_4$). DOTA-OSu (5.0 mg, 10.0 μmol) and 6P-RGK$_4$ (3.8 mg, 0.9 μmol) were dissolved in DMF (1 mL). After addition of DIEA (3 drops), the reaction mixture was stirred for 2 h at room temperature. Upon addition of 2 mL NH$_4$OAc buffer (100 mM, pH = 7.0), the product was separated from the mixture by HPLC (Method 1). Lyophilization of the collected fraction at ~18.6 min afforded DOTA-6P-RGK$_4$ with >95% HPLC purity. The yield was 2.8 mg (~68%). MALDI-MS: m/z = 4622.7 for $[M + H]^+$ (M = 4618.1 calcd. for $[C_{205}H_{331}N_{49}O_{71}]^+$).

[111]In-Labeling. To a clean Eppendorf tube were added 200 μL of the DOTA conjugate solution (2.5 mg/mL in 0.1 M NaOAc buffer, pH = 5.5) and 20 μL of

[111]InCl$_3$ solution (~500 μCi in 0.05 M HCl). The vial was heated in a water bath at 100 °C for ~ 15 min. After cooling to room temperature, a sample of the resulting solution was analyzed by radio-HPLC (Method 2). The water-octanol partition coefficients of all ^{111}In radiotracers were determined according to literature methods [40, 41]. The log P values were reported as an average of three independent measurements plus the standard deviation.

Dose Preparation. For biodistribution studies, all new ^{111}In radiotracers were purified by HPLC (Method 2). Volatiles in the HPLC mobile phase were removed under vacuum (~5 mmHg) at room temperature. Doses were prepared by dissolving the ^{111}In radiotracer in saline to 70 – 100 μCi/mL. For the blocking experiment, excess RGD$_2$ was dissolved in the dose solution to 7.5 mg/mL. For planar imaging studies, doses were prepared by dissolving the radiotracer (no purification) in saline to ~1 mCi/mL. In all cases, the dose solution was filtered with a 0.20 μm Millex-LG filter before being injected into the animals. Each animal was injected with ~0.1 mL of the dose solution.

In Vitro Whole-Cell Integrin $\alpha_v\beta_3$ Binding Assay. The integrin binding affinity and specificity of cyclic RGD peptides were assessed using ^{125}I-c(RGDyK) as the integrin-specific radioligand. Briefly, U87MG human glioma cells were grown in Gibco's Dulbecco's medium supplemented with 10% fetal bovine serum (FBS), 100 IU/ml penicillin and 100 μg/ml streptomycin (Invitrogen Co, Carlsbad, CA), at 37 °C in humidified atmosphere containing 5% CO$_2$. Filter multiscreen DV plates were seeded with 10^5 glioma cells in binding buffer and incubated with ^{125}I-c(RGDyK) in the presence of increasing concentrations of the RGD conjugate. After removing the unbound ^{125}I-c(RGDyK), hydrophilic PVDF filters were collected. The radioactivity was determined using a γ-counter (Packard, Meriden, CT). The IC$_{50}$ values were calculated by fitting the data by nonlinear regression using GraphPad Prism™ (GraphPad Software, Inc., San Diego, CA). Experiments were carried out twice with triplicate samples. IC$_{50}$ values are reported as an average plus the standard deviation.

Animal Model. Biodistribution and imaging studies were performed using the athymic nude mice bearing U87MG human glioma xenografts in compliance with NIH animal experiment guidelines (*Principles of Laboratory Animal Care*, NIH Publication No. 86-23, revised 1985). The animal protocol has been approved by the Purdue University Animal Care and Use Committee. U87MG cells were cultured in the Minimum Essential Medium, Eagle with Earle's Balanced Salt Solution (non-essential amino acids sodium

pyruvate) (ATCC, Manassas, VA) in humidified atmosphere of 5% carbon dioxide, and were supplemented with 10% fetal bovine serum and 1% penicillin and streptomycin solution (GIBCO, Grand Island, NY). Female athymic nu/nu mice were purchased from Harlan (Indianapolis, IN) at 4 – 5 weeks of age. Each mouse was implanted subcutaneously with ~5 × 10^6 U87MG tumor cells into the left and right upper flanks. In this way, one could assess the impact of tumor size on the radiotracer imaging quality in a single tumor-bearing mouse. All procedures were performed in a laminar flow cabinet using aseptic technique. Four weeks after inoculation, the tumor size was 0.1 – 0.4 g, and animals were used for biodistribution and imaging studies.

Biodistribution Protocol. Twenty-five tumor-bearing mice (20 – 25 g) were randomly divided into five groups. Each tumor-bearing mouse was administered with ~3 µCi of the ^{111}In radiotracer by tail vein injection. Five animals were sacrificed by sodium pentobarbital overdose (~200 mg/kg) at 0.5, 1, 4, 24 and 72 h postinjection (p.i.). Blood samples were withdrawn from the heart of tumor-bearing mice. The tumor and normal organs (brain, eyes, heart, spleen, lungs, liver, kidneys, muscle and intestine) were harvested, washed with saline, dried with absorbent tissue, weighed, and counted on a Perkin Elmer Wizard – 1480 γ-counter (Shelton, CT). The organ uptake was calculated as the percentage of injected dose per gram of organ mass (%ID/g) or the percentage of injected dose per organ (%ID/organ). For the blocking experiment, five tumor-bearing athymic nude mice (20 – 25 g) were used, and each animal was administered with ~3 µCi of ^{111}In(DOTA-6P-RGD$_4$) along with ~350 µg (~14 mg/kg) of RGD$_2$. Such a high dose of RGD$_2$ was used to make sure that the integrin α$_v$β$_3$ binding was completely blocked. At 1 h p.i., all five tumor-bearing animals were sacrificed for organ biodistribution. Biodistribution data (%ID/g) and target-to-background (T/B) ratios are reported as an average plus the standard deviation based on the results from five tumor-bearing mice (10 tumors) at each time point. Comparison between two radiotracers was made using the two-way ANOVA test (GraphPad Prim 5.0, San Diego, CA). The level of significance was set at $p < 0.05$.

Tissue Immunohistochemistry. The xenografted U87MG tumor and normal organ (lung, liver and kidney) tissues were harvested from the tumor-bearing mice. Tissues were immediately snap-frozen in OCT (optical cutting temperature) solution and cut into 5 µm-thick slices. After thorough drying at room temperature, the slides were fixed with ice-cold acetone for 10 min. The sections were then blocked and incubated with anti-integrin β$_3$ antibody (1:100, Santa Cruz) and CD31 antibody (1:100, BD Biosciences) for 1 h at room temperature. After washing, DyLight 594- and fluorescein isothiocyanate (FITC)-conjugated second antibodies (1:500, Jackson ImmunoResearch Inc., West Grove, PA) were added to link to integrin β$_3$ or CD31 primary antibody, respectively. The fluorescence was visualized with an Olympus BX51 fluorescence microscope (Olympus America Inc., Center Valley, PA). Phase contrast pictures were also obtained as the histological reference to illustrate the texture of the tumor or normal organ tissue and demonstrate the site of fluorescent staining. All the pictures were taken under 100x magnification. The same procedure was used to compare integrin β$_3$ expression levels in the U87MG tumor, kidneys, liver and lungs.

Western Blot. The xenografted U87MG glioma tumor tissue and normal organ tissues (lung, liver and kidney) were excised and homogenized in the RIPA buffer. Protease inhibitors were added freshly into the lysis buffer before experiments. After sonication, lysates were centrifuged at 12,000 g at 4 °C for 15 min. The protein concentration was determined using the Bio-Rad Protein Assay Reagent (Bio-Rad Laboratories Inc., Hercules, CA). The protein lysates (50 µg) were separated by 10% SDS-PAGE and transferred to PVDF membranes for detection of integrin β$_3$. The blots were incubated in blocking solution consisting of 5% milk and 3% BSA in TBS-T for 1 h at room temperature and then were immunoblotted at room temperature for 2 h with the rabbit polyclonal anti-β3 primary antibody (1:1000, Cell Signaling Technology, Danvers, MA). The anti-rabbit secondary antibody was incubated with the blots for another 1 h at room temperature. Detection by enzyme-linked chemiluminescence was performed according to the manufacturer's protocol (Thermo Fisher Scientific, Rockford, IL).

Planar Imaging. The imaging studies were performed on ^{111}In(DOTA-2P-RGD$_4$), ^{111}In(DOTA-2P4G-RGD$_4$) and ^{111}In(DOTA-6P-RGD$_4$) using the athymic nude mice (n = 3) bearing U87MG human glioma xenografts. Each tumor-bearing mouse was administered with ~100 µCi of ^{111}In radiotracer in 0.1 mL saline via tail vein injection. Animals were anesthetized with intraperitoneal injection of ketamine (80 mg/kg) and xylazine (19 mg/kg), and were then placed supine on a single head mini gamma camera (Diagnostic Services Inc., NJ) equipped with a parallel-hole, medium-energy and high-resolution collimator. The whole-body anterior images were acquired at 0.5, 1, 4, 24 and 72 h p.i. and stored digitally in a 128 x 128 matrix. The acquisition count limits were set at 200 K. After completion of imaging, animals were sacrificed

by sodium pentobarbital overdose (~200 mg/kg).

Metabolism. Athymic nude mice were used for metabolism studies. Each mouse was administered with ~100 μCi of [111]In(DOTA-2P-RGD$_4$), [111]In(DOTA-2P4G-RGD$_4$) and [111]In(DOTA-6P-RGD$_4$) via tail vein. The urine samples were collected at 30 min and 120 min p.i. by manual void, and were mixed with equal volume of 50% acetonitrile aqueous solution. The mixture was centrifuged at 8,000 rpm for 5 min at room temperature. The supernatant was collected and passed through a 0.20 micron Millex-LG filter unit to remove any precipitate or particles. The filtrate was analyzed by radio-HPLC (Method 2). The feces samples were collected at 120 min p.i. and suspended in a mixture of 20% acetonitrile aqueous solution (2 mL). The resulting mixture was vortexed for 10 min. After centrifuging at 8,000 rpm for 5 min, the supernatant was collected and passed through a 0.20 μm Millex-LG filter unit. The filtrate was analyzed by radio-HPLC (Method 2). The kidney and liver tissues were harvested at 120 min p.i., counted in a Perkin Elmer Wizard – 1480 γ-counter (Shelton, CT) for total radioactivity, and then homogenized. The homogenate was mixed with 2 mL 20% acetonitrile aqueous solution. After centrifuging at 8,000 rpm for 5 min, the supernatant was collected and counted on a γ-counter to determine the percentage of radioactivity recovery. After filtration through a 0.20 μm Millex-LG filter unit to remove foreign particles or precipitate, the filtrate was then analyzed by radio-HPLC (Method 2). The percentage of radioactivity recovery was >95% (by γ-counting) for both urine and feces samples.

Results

Cyclic RGD Conjugates. Syntheses of DOTA-P-RGD and DOTA-P-RGD$_2$ were straightforward by conjugation of DOTA-OSu with PEG$_4$-c(RGDfK) and PEG$_4$-E[c(RGDfK)]$_2$, respectively, in DMF in the presence of excess DIEA. The key step for successful preparation of DOTA-2P-RGD$_4$, DOTA-2P4G-RGD$_4$ and DOTA-6P-RGD$_4$ was the deprotection of Boc-2P-RGD$_4$, Boc-2P4G-RGD$_4$ and Boc-6P-RGD$_4$, respectively. In general, excess TFA must be removed within 10 min of the reaction in order to minimize formation of hydrolyzed products. Conjugation of 2P-RGD$_4$, 2P4G-RGD$_4$ and 6P-RGD$_4$ with DOTA-OSu in anhydrous DMF afforded their corresponding conjugates DOTA-2P-RGD$_4$, DOTA-2P4G-RGD$_4$ and DOTA-6P-RGD$_4$, respectively. DOTA-6P-RGK$_4$ was prepared using the identical procedure to that for DOTA-6P-RGD$_4$. DOTA-6P-RGK$_4$ has the identical amino acids, but their sequence was scrambled to demonstrate the RGD-specificity of DOTA-6P-RGD$_4$. The identities for all new RGD conjugates were confirmed by ESI-MS (positive mode) or MALDI-MS. Their HPLC purity was >95% before being used for ^{111}In-labeling and determination of their integrin $\alpha_v\beta_3$ binding affinity.

Integrin $\alpha_v\beta_3$ Binding Affinity. Figure 2 shows the displacement curves of ^{125}I-c(RGDyK) bound to U87MG glioma cells in the presence of cyclic RGD peptides. Their IC$_{50}$ values were obtained from curve fitting from Figure 2, and were calculated to be 49.9 ± 5.5, 44.3 ± 3.5, 5.0 ± 1.0, 1.5 ± 0.2, 0.5 ± 0.1, 0.2 ± 0.1, 0.3 ± 0.1, and 437 ± 35 nM for c(RGDfK), DOTA-P-RGD, DOTA-P-RGD$_2$, DOTA-3P-RGD$_2$, DOTA-2P-RGD$_4$, DOTA-2P4G-RGD$_4$, DOTA-6P-RGD$_4$ and DOTA-6P-RGK$_4$, respectively. DOTA-6P-RGK$_4$ has much lower binding affinity than DOTA-6P-RGD$_4$ (Figure 2). The IC$_{50}$ of DOTA-3P-RGD$_2$ was almost identical to that (IC$_{50}$ = 1.3 ± 0.2 nM) presented in our previous report [45].

Radiochemistry. All ^{111}In radiotracers were prepared by reacting [111]InCl$_3$ with the respective DOTA conjugates (DOTA-P-RGD, DOTA-P-RGD$_2$, DOTA-2P-RGD$_4$, DOTA-2P4G-RGD$_4$, DOTA-6P-RGD$_4$ and DOTA-6P-RGK$_4$) in NH$_4$OAc buffer (100 mM, pH = 5.5). Radiolabeling was completed by heating the reaction mixture at 100 °C for ~15 min. The radiochemical purity was >95% with the specific activity of > 40 mCi/μmol for all ^{111}In radiotracers. Their HPLC retention times and log P values were listed in Table 1. We found that all new ^{111}In radiotracers remain stable for more than 72 h in the kit matrix or after HPLC purification in the presence of 3 mM EDTA.

Biodistribution Characteristics. Selected biodistribution data for [111]In(L) (L = DOTA-P-RGD, DOTA-P-RGD$_2$, DOTA-2P-RGD$_4$, DOTA-2P4G-RGD$_4$, DOTA-6P-RGD$_4$ and DOTA-6P-RGK$_4$) are listed in Tables 2-6. Figure 3 compares their uptake (%ID/g) in the tumor and intestine, as well as their tumor/kidney and tumor/liver ratios in athymic nude mice (n = 5) bearing U87MG glioma xenografts. The biodistribution data and T/B ratios for [111]In(DOTA-3P-RGD$_3$) and [111]In(DOTA-6G-RGD$_4$) were obtained from our previous reports [45, 46]. The comparison of their tumor uptake will allow us to determine if the cyclic RGD tetramers (DOTA-2P-RGD$_4$, DOTA-2P4G-RGD$_4$ and DOTA-6P-RGD$_4$) are actually tetravalent in binding to integrin $\alpha_v\beta_3$.
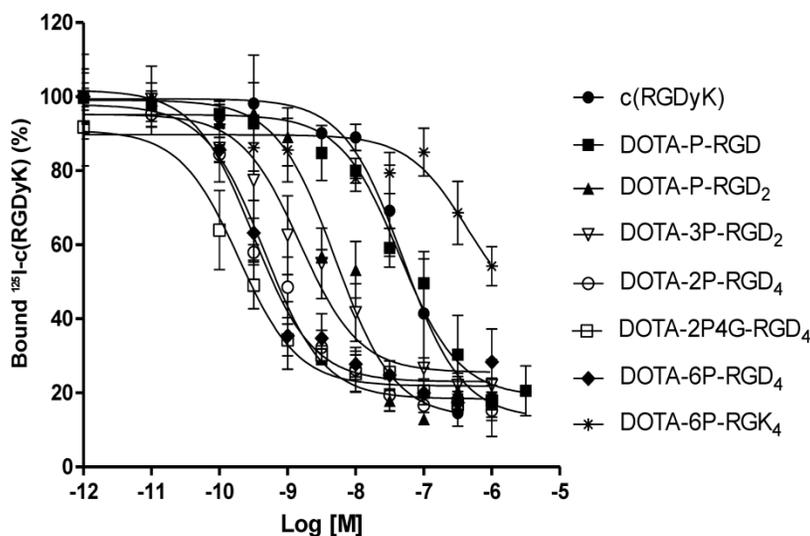
Figure 2. Competitive inhibition curves of ^{125}I-c(RGDyK) bound to the U87MG human glioma cells by c(RGDyK), DOTA-P-RGD, DOTA-P-RGD$_2$, DOTA-3P-RGD$_2$, DOTA-2P-RGD$_4$, DOTA-2P4G-RGD$_4$, DOTA-6P-RGD$_4$ and DOTA-6P-RGK$_4$. Their IC$_{50}$ values were calculated to be 49.9 ± 5.5, 44.3 ± 3.5, 5.0 ± 1.0, 1.5 ± 0.2, 0.5 ± 0.1, 0.2 ± 0.1, 0.3 ± 0.1, and 437 ± 35 nM, respectively. The integrin $\alpha_v\beta_3$ binding affinity follows the order: DOTA-6P-RGD$_4$ ~ DOTA-2P4G-RGD$_4$ ~ DOTA-2P-RGD$_4$ > DOTA-3P-RGD$_2$ **>** DOTA-P-RGD$_2$ > DOTA-P-RGD >> DOTA-6P-RGK$_4$.
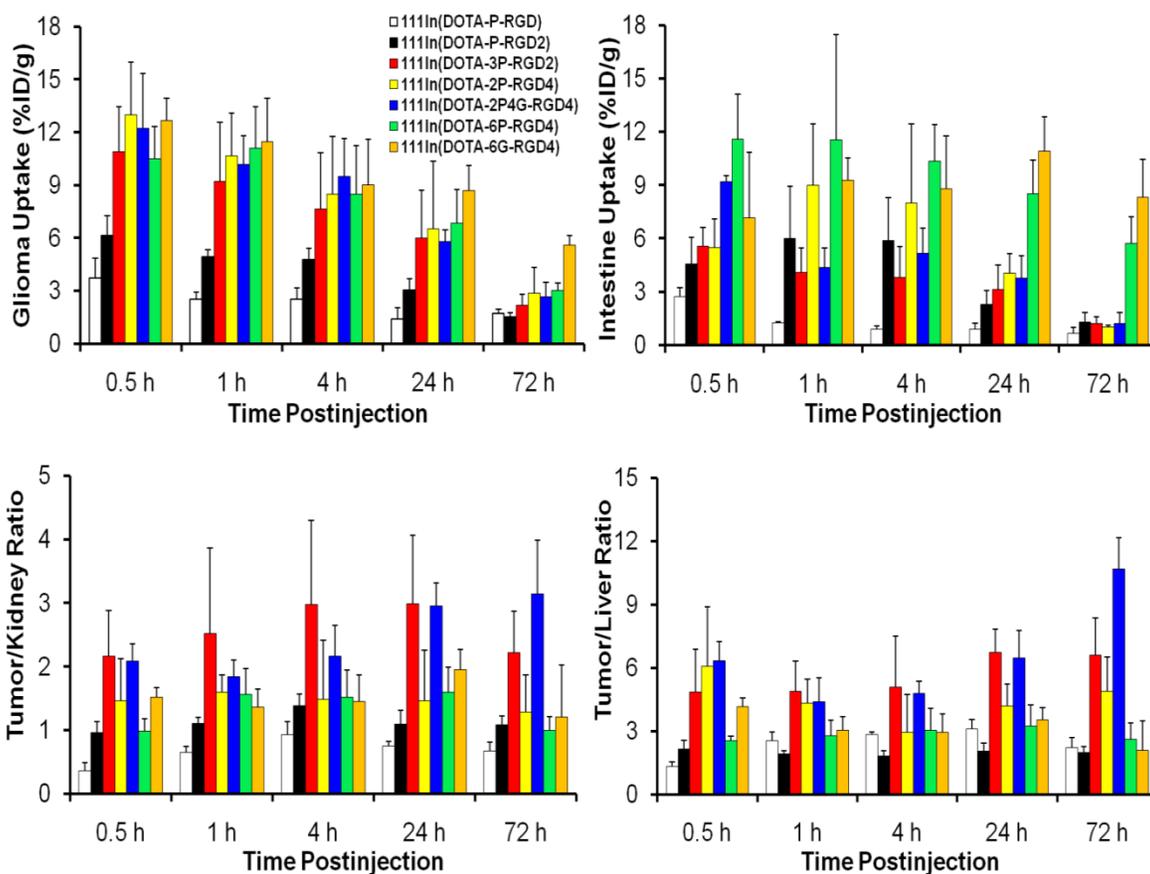
Figure 3. Comparison of the uptake (%ID/g) in tumor and intestine, as well as the tumor/kidney and tumor/liver ratios for ^{111}In(L) (L = DOTA-P-RGD, DOTA-P-RGD$_2$, DOTA-3P-RGD$_2$, DOTA-2P-RGD$_4$, DOTA-2P4G-RGD$_4$, DOTA-6P-RGD$_4$ and DOTA-6G-RGD$_4$) in the athymic nude mice (n = 5) bearing U87MG glioma xenografts. Biodistribution data and T/B ratios for ^{111}In(DOTA-3P-RGD$_3$) and ^{111}In(DOTA-6G-RGD$_4$) were obtained from our previous reports [45, 46].

Table 1. Radiochemical purity (RCP), HPLC retention time and log P values for ^{111}In-labeled cyclic RGD peptides.

Radiotracer	RCP (%)	Retention Time (min)	Log P Value
[111]In(DOTA-P-RGD)	> 95	12.4	-3.48 ± 0.12
[111]In(DOTA-P-RGD$_2$)	> 92	16.7	-3.22 ± 0.09
[111]In(DOTA-3P-RGD$_2$)	> 97	19.6	-4.20 ± 0.21
[111]In(DOTA-2P-RGD$_4$)	> 97	19.7	-3.87 ± 0.11
[111]In(DOTA-2P4G-RGD$_4$)	> 95	18.4	-3.93 ± 0.09
[111]In(DOTA-6P-RGD$_4$)	> 95	19.9	-3.68 ± 0.03
[111]In(DOTA-6P-RGK$_4$)	> 95	19.1	-3.61 ± 0.07

Table 2. Selected Biodistribution data of [111]In(DOTA-P-RGD) in athymic nude mice (n = 5) bearing U87MG human glioma xenografts.

%ID/gram	0.5 h	1 h	4 h	24 h	72 h
Blood	7.39 ± 0.78	0.63 ± 0.03	0.29 ± 0.02	0.06 ± 0.00	0.02 ± 0.01
Brain	0.27 ± 0.02	0.08 ± 0.02	0.04 ± 0.01	0.03 ± 0.00	0.02 ± 0.00
Eyes	0.85 ± 0.15	0.48 ± 0.20	0.24 ± 0.01	0.14 ± 0.01	0.10 ± 0.01
Heart	1.83 ± 0.08	0.40 ± 0.03	0.27 ± 0.03	0.14 ± 0.01	0.09 ± 0.01
Intestine	2.72 ± 0.50	1.24 ± 0.09	0.91 ± 0.16	0.91 ± 0.33	0.67 ± 0.32
Kidney	10.94 ± 3.96	3.93 ± 0.09	2.80 ± 0.29	1.92 ± 0.16	1.07 ± 0.11
Liver	2.79 ± 0.02	1.00 ± 0.08	0.90 ± 0.15	0.47 ± 0.07	0.30 ± 0.07
Lungs	4.60 ± 0.39	1.01 ± 0.05	0.59 ± 0.01	0.30 ± 0.06	0.16 ± 0.03
Muscle	1.20 ± 0.35	0.38 ± 0.05	0.27 ± 0.03	0.19 ± 0.04	0.13 ± 0.05
Spleen	2.91 ± 0.51	0.83 ± 0.10	0.73 ± 0.16	0.63 ± 0.11	0.37 ± 0.05
U87MG	3.74 ± 0.55	2.54 ± 0.37	2.56 ± 0.40	1.43 ± 0.09	0.74 ± 0.16
Tumor/Blood	0.52 ± 0.10	4.04 ± 0.70	8.75 ± 1.74	23.72 ± 1.84	40.06 ± 16.44
Tumor /Brain	13.79 ± 1.72	36.49 ± 13.29	73.08 ± 3.00	50.63 ± 5.24	37.16 ± 10.39
Tumor /Heart	2.06 ± 0.32	6.36 ± 1.25	9.51 ± 1.48	9.91 ± 0.73	7.62 ± 1.67
Tumor /Kidney	0.36 ± 0.13	0.65 ± 0.10	0.93 ± 0.20	0.75 ± 0.07	0.67 ± 0.15
Tumor /Liver	1.34 ± 0.20	2.55 ± 0.42	2.83 ± 0.14	3.10 ± 0.47	2.22 ± 0.48
Tumor /Lungs	0.83 ± 0.14	2.54 ± 0.45	4.36 ± 0.68	4.90 ± 1.02	4.66 ± 1.02
Tumor /Muscle	3.46 ± 1.23	6.89 ± 1.55	9.50 ± 1.31	7.90 ± 1.41	7.12 ± 2.37

Table 3. Selected Biodistribution data of [111]In(DOTA-P-RGD$_2$) in athymic nude mice (n = 5) bearing U87MG human glioma xenografts.

%ID/gram	0.5 h	1 h	4 h	24 h	72 h
Blood	1.13 ± 0.13	0.51 ± 0.09	0.22 ± 0.05	0.07 ± 0.02	0.03 ± 0.01
Bone	1.52 ± 0.47	1.12 ± 0.14	0.70 ± 0.18	0.79 ± 0.11	0.43 ± 0.06
Brain	0.11 ± 0.02	0.10 ± 0.02	0.09 ± 0.05	0.06 ± 0.00	0.03 ± 0.01
Eyes	0.94 ± 0.18	0.82 ± 0.27	0.62 ± 0.22	0.39 ± 0.12	0.20 ± 0.04
Heart	1.03 ± 0.26	0.69 ± 0.19	0.56 ± 0.15	0.35 ± 0.05	0.14 ± 0.02
Intestine	4.58 ± 1.49	5.99 ± 2.93	5.88 ± 2.42	2.28 ± 0.78	1.30 ± 0.52
Kidney	6.36 ± 0.80	4.45 ± 0.21	3.44 ± 0.43	2.79 ± 0.33	1.44 ± 0.13
Liver	2.84 ± 0.36	2.57 ± 0.42	2.60 ± 0.37	1.51 ± 0.57	0.78 ± 0.34
Lungs	3.01 ± 0.43	1.91 ± 0.25	1.52 ± 0.75	0.78 ± 0.09	0.33 ± 0.04
Muscle	1.17 ± 0.26	0.80 ± 0.24	0.70 ± 0.41	0.39 ± 0.11	0.24 ± 0.10
Spleen	2.01 ± 0.43	1.65 ± 0.13	1.75 ± 0.27	1.47 ± 0.35	0.58 ± 0.09
U87MG	6.14 ± 1.12	4.95 ± 0.39	4.79 ± 0.61	3.08 ± 0.60	1.55 ± 0.21
Tumor/Blood	5.43 ± 0.99	9.80 ± 0.78	22.00 ± 2.79	41.34 ± 8.03	53.22 ± 6.41
Tumor/Kidney	0.96 ± 0.18	1.11 ± 0.09	1.39 ± 0.18	1.10 ± 0.21	1.08 ± 0.14
Tumor/Liver	2.16 ± 0.39	1.92 ± 0.15	1.84 ± 0.23	2.04 ± 0.40	2.00 ± 0.26
Tumor/Lungs	2.04 ± 0.37	2.60 ± 0.21	3.15 ± 0.40	3.95 ± 0.77	4.75 ± 0.63
Tumor/Muscle	5.22 ± 0.95	6.18 ± 0.49	6.88 ± 0.87	7.90 ± 1.53	6.36 ± 0.84

Table 4. Selected biodistribution data of ^{111}In(DOTA-2P-RGD$_4$) in athymic nude mice (n = 5) bearing U87MG human glioma xenografts.

%ID/gram	0.5 h	1 h	4 h	24 h	72 h
Blood	1.12 ± 0.08	0.31 ± 0.16	0.05 ± 0.02	0.03 ± 0.00	0.02 ± 0.02
Bone	1.89 ± 0.37	1.83 ± 0.70	1.46 ± 0.69	84 ± 0.34	0.34 ± 0.03
Brain	0.10 ± 0.01	0.12 ± 0.04	0.07 ± 0.03	0.05 ± 0.01	0.02 ± 0.01
Eyes	0.87 ± 0.24	1.10 ± 0.22	0.78 ± 0.31	0.39 ± 0.12	0.21 ± 0.12
Heart	1.12 ± 0.20	0.86 ± 0.22	0.68 ± 0.31	0.31 ± 0.12	0.10 ± 0.01
Intestine	5.50 ± 1.61	8.98 ± 3.47	7.98 ± 4.47	4.04 ± 1.11	1.03 ± 0.10
Kidney	8.89 ± 1.28	6.67 ± 1.01	5.68 ± 0.66	4.38 ± 1.10	2.31 ± 0.61
Liver	2.13 ± 0.74	2.39 ± 0. 97	2.89 ± 1.36	1.56 ± 0.37	0.55 ± 0.05
Lungs	3.19 ± 0.78	2.47 ± 0.66	1.93 ± 0.77	0.96 ± 0.33	0.33 ± 0.03
Muscle	0.93 ± 0.29	0.91 ± 0.37	0.72 ± 0.23	0.39 ± 0.26	0.12 ± 0.04
Spleen	2.36 ± 0.96	2.47 ± 0.66	1.98 ± 0.97	1.22 ± 0.44	0.36 ± 0.02
U87MG	12.98 ± 5.99	10.66 ± 2.41	8.49 ± 5.28	6.52 ± 3.85	2.87 ± 1.45
Tumor/Blood	11.60 ± 5.36	34.67 ± 7.84	161.22 ± 100.35	231.33 ± 136.67	192.06 ± 172.1
Tumor /Kidney	1.46 ± 0.67	1.60 ± 0.27	1.49 ± 0.93	1.46 ± 0.80	1.28 ± 0.59
Tumor /Liver	6.09 ± 2.81	4.34 ± 1.12	2.93 ± 1.82	4.19 ± 1.04	4.89 ± 1.62
Tumor /Lungs	4.06 ± 1.88	4.31 ± 0.96	4.40 ± 2.74	6.76 ± 3.99	8.94 ± 5.37
Tumor /Muscle	13.92 ± 6.43	11.76 ± 3.58	11.83 ± 7.36	16.78 ± 9.92	25.87 ± 15.57

Table 5. Selected biodistribution data of ^{111}In(DOTA-2P4G-RGD$_4$) in athymic nude mice (n = 5) bearing U87MG human glioma xenografts.

%ID/gram	0.5 h	1 h	4 h	24 h	72 h
Blood	0.84 ± 0.32	0.13 ± 0.00	0.04 ± 0.00	0.02 ± 0.00	0.03 ± 0.01
Bone	2.17 ± 0.42	1.76 ± 0.26	1.24 ± 0.16	0.84 ± 0.10	0.42 ± 0.11
Brain	0.20 ± 0.10	0.07 ± 0.00	0.06 ± 0.02	0.04 ± 0.01	0.04 ± 0.02
Eyes	1.33 ± 0.23	0.69 ± 0.07	0.66 ± 0.08	0.31 ± 0.01	0.35 ± 0.24
Heart	1.79 ± 0.31	0.61 ± 0.04	0.57 ± 0.06	0.26 ± 0..02	0.13 ± 0.01
Intestine	10.36 ± 1.52	4.35 ± 1.13	5.18 ± 1.39	3.78 ± 1.23	1.22 ± 0.61
Kidney	10.72 ± 2.13	5.57 ± 0.63	4.40 ± 0.63	1.98 ± 0.31	0.85 ± 0.09
Liver	3.62 ± 0.85	2.36 ± 0.27	1.98 ± 0.39	0.91 ± 0.08	0.25 ± 0.06
Lungs	4.26 ± 0.78	2.38 ± 0.28	1.91 ± 0.27	1.04 ± 0.04	0.30 ± 0.03
Muscle	1.64 ± 0.42	0.98 ± 0.11	0.52 ± 0.07	0.30 ± 0.16	0.27 ± 0.07
Spleen	2.97 ± 0.61	2.02 ± 0.34	1.54 ± 0.25	1.06 ± 0.19	0.54 ± 0.22
U87MG	11.43 ± 2.92	10.18 ± 1.61	9.50 ± 2.13	5.79 ± 0.67	2.66 ± 0.81
Tumor/Blood	13.58 ± 3.47	80.74 ± 10.67	218.26 ± 44.57	266.19 ± 59.02	93.96 ± 22.32
Tumor/Bone	5.27 ± 1.35	5.80 ± 0.65	7.87 ± 2.44	7.02 ± 1.39	6.76 ± 2.74
Tumor /Kidney	1.07 ± 0.27	1.84 ± 0.26	2.17 ± 0.48	2.96 ± 0.36	3.14 ± 0.84
Tumor /Liver	3.15 ± 0.81	4.39 ± 1.13	4.79 ± 0.58	6.46 ± 1.33	10.71 ± 1.45
Tumor /Lungs	2.68 ± 0.69	4.38 ± 1.28	5.07 ± 1.52	5.59 ± 0.63	8.73 ± 1.70
Tumor /Muscle	6.99 ± 1.79	10.43 ± 1.75	18.07 ± 2.95	24.04 ± 14.24	10.16 ± 2.72

Table 6. Selected biodistribution data of ^{111}In(DOTA-6P-RGD$_4$) in athymic nude mice (n = 5) bearing U87MG human glioma xenografts.

%ID/gram	0.5 h	1 h	4 h	24 h	72 h
Blood	0.92 ± 0.06	0.29 ± 0.14	0.20 ± 0.02	0.12 ± 0.02	0.06 ± 0.00
Bone	1.27 ± 0.23	1.20 ± 0.19	089 ± 0.14	0.88 ± 0.03	0.66 ± 0.01
Brain	0.15 ± 0.01	0.14 ± 0.03	0.12 ± 0.01	0.08 ± 0.01	0.09 ± 0.06
Eyes	2.78 ± 2.01	1.43 ± 0.25	1.03 ± 0.14	0.63 ± 0.10	0.48 ± 0.06
Heart	0.57 ± 0.15	0.78 ± 0.24	0.44 ± 0.04	0.55 ± 0.06	0.37 ± 0.07
Intestine	11.60 ± 2.52	11.53 ± 6.94	10.36 ± 2.03	8.53 ± 1.88	5.74 ± 1.47

Kidney	10.68 ± 1.79	7.21 ± 0.79	5.55 ± 0.88	4.27 ± 0.22	3.10 ± 0.38
Liver	4.09 ± 0.54	4.01 ± 0.41	2.82 ± 0.54	1.50 ± 0.17	1.23 ± 0.27
Lungs	4.06 ± 0.88	3.69 ± 0.92	2.18± 0.26	1.62 ± 0.21	0.66 ± 0.08
Muscle	1.79 ± 0.11	1.04 ± 0.20	0.67 ± 0.09	0.52 ± 0.05	0.23 ± 0.05
Spleen	2.69 ± 0.63	2.12± 0.20	2.07 ± 0.37	1.67 ± 0.18	1.12 ± 0.15
U87MG	10.48 ± 1.83	11.08 ± 2.38	8.48 ± 2.75	6.86 ± 1.87	3.04 ± 0.39
Tumor/Blood	11.32 ± 1.71	46.41 ± 25.60	42.10 ± 16.02	56.45 ± 10.80	52.90 ± 4.95
Tumor /Kidney	0.99 ± 0.19	1.56 ± 0.41	1.52 ± 0.43	1.60 ± 0.39	1.00 ± 0.21
Tumor /Liver	2.55 ± 0.21	2.79 ± 0.73	3.04 ± 1.03	3.24 ± 1.02	2.60 ± 0.80
Tumor /Lungs	2.61 ± 0.33	3.13 ± 1.09	3.86 ± 1.09	4.68 ± 1.72	4.70 ± 0.86
Tumor /Muscle	5.83 ± 0.80	10.90 ± 2.51	12.56 ± 3.70	13.09 ± 2.85	13.47 ± 3.64

In the glioma model, ^{111}In(DOTA-6P-RGD$_4$) was excreted mainly via renal route with >75% of the injected radioactivity recovered from urine and <10% of the injected radioactivity from feces. ^{111}In(DOTA-6P-RGD$_4$) had a rapid blood clearance with high tumor/blood ratios (Table 6). It had a high initial tumor uptake (10.5 %ID/g at 0.5 h p.i.) with a slow tumor radioactivity washout ($t_{1/2} \sim 40$ h). ^{111}In(DOTA-6P-RGD$_4$) had a moderately low liver uptake with high tumor/liver ratio (Table 6). However, ^{111}In(DOTA-6P-RGD$_4$) had significant uptake in kidneys and intestine. Similar results were also obtained for ^{111}In(DOTA-6G-RGD$_4$) in the same animal model [46]. ^{111}In(DOTA-2P4G-RGD$_4$) was also excreted through the renal route with >80% of the injected radioactivity recovered from urine samples. ^{111}In(DOTA-2P4G-RGD$_4$) had a rapid blood clearance with high tumor/blood ratios (Table 5). The initial tumor uptake of ^{111}In(DOTA-2P4G-RGD$_4$) (11.4 %ID/g at 0.5 h p.i.) was comparable to that of ^{111}In(DOTA-6P-RGD$_4$) (10.5 %ID/g at 0.5 h p.i.) within the experimental error; but its tumor radioactivity washout was slightly faster with $t_{1/2}$ being ~35 h. ^{111}In(DOTA-2P4G-RGD$_4$) also showed high tumor/muscle ratio (Table 5), and a rapid liver clearance (3.6 and 0.25 %ID/g at 0.5 and 72 h p.i., respectively). As a result, ^{111}In(DOTA-2P4G-RGD$_4$) has the highest tumor/liver ratio at 72 h p.i. (Figure 3). ^{111}In(DOTA-2P4G-RGD$_4$) also had very high initial intestine uptake; but it was much lower (p <0.01) than that of ^{111}In(DOTA-6P-RGD$_4$) at >1 h p.i. The tumor uptake of ^{111}In(DOTA-2P-RGD$_4$) was also high and close to that of ^{111}In(DOTA-6P-RGD$_4$) over the 72 h period (Figure 3). Its intestine uptake was comparable to that of ^{111}In(DOTA-6P-RGD$_4$) within the experimental errors (Figure 3). ^{111}In(DOTA-2P-RGD$_4$) had a rapid clearance from normal organs, such as the blood, kidneys and liver. The tumor/liver and tumor/kidney ratios of ^{111}In(DOTA-2P-RGD$_4$) were well comparable to those obtained for ^{111}In(DOTA-6P-RGD$_4$) and ^{111}In(DOTA-6G-RGD$_4$) (Figure 3).

It seems that ^{111}In(DOTA-2P-RGD$_4$), ^{111}In(DOTA-2P4G-RGD$_4$) and ^{111}In(DOTA-6P-RGD$_4$) might have higher tumor uptake than ^{111}In(DOTA-3P-RGD$_2$) over the first 24 h, but their tumor uptake differences were not significant within the experimental error ($p > 0.05$). The 72 h tumor uptake follows the general order of ^{111}In(DOTA-6P-RGD$_4$) (3.04 %ID/g) > ^{111}In(DOTA-2P-RGD$_4$) (2.87 %ID/g) ~ ^{111}In(DOTA-2P4G-RGD$_4$) (2.66 %ID/g) > ^{111}In(DOTA-3P-RGD$_2$) (2.18 %ID/g), which is similar to the trend of integrin $\alpha_v\beta_3$ binding affinity of DOTA-6P-RGD$_4$ (IC$_{50}$ = 0.3 ± 0.1 nM) ~ DOTA-2P4G-RGD$_4$ (IC$_{50}$ = 0.2 ± 0.1 nM) ~ DOTA-2P-RGD$_4$ (IC$_{50}$ = 0.5 ± 0.1 nM) > DOTA-3P-RGD$_2$ (IC$_{50}$ = 1.5 ± 0.2 nM). Among the ^{111}In radiotracers evaluated in this animal model, ^{111}In(DOTA-6G-RGD$_4$) had the highest uptake in the tumor and intestine (Figure 3) at 72 h p.i. The half-life of ^{111}In(DOTA-6G-RGD$_4$) in the tumor was estimated to be 60 h. In contrast, ^{111}In(DOTA-3P-RGD$_2$) and ^{111}In(DOTA-2P4G-RGD$_4$) had low uptake in the intestine, kidneys and liver over the 72 h period. This was particularly true at > 24 h p.i. As a result, ^{111}In(DOTA-3P-RGD$_2$) and ^{111}In(DOTA-2P4G-RGD$_4$) had the tumor/kidney and tumor/liver ratios that were significantly better ($p < 0.05$) than those of ^{111}In(DOTA-6G-RGD$_4$) and ^{111}In(DOTA-6P-RGD$_4$) during that period of time (Figure 3).

As expected, ^{111}In(DOTA-P-RGD) had the lowest tumor uptake (3.7 and 0.7 %ID/g at 0.5 and 72 h p.i., respectively) among ^{111}In radiotracers evaluated in this study. ^{111}In(DOTA-P-RGD$_2$) had a relatively high tumor uptake (6.1 at 0.5 h p.i.), but it had a significant washout from the tumor with uptake values being 4.9, 4.8, 3.1 and 1.6 %ID/g at 1, 4, 24 and 72 h p.i., respectively. The tumor uptake follows the trend of ^{111}In(DOTA-3P-RGD$_2$) > ^{111}In(DOTA-P-RGD$_2$) > ^{111}In(DOTA-P-RGD), which is completely consistent with the order of their $\alpha_v\beta_3$ binding affinity (IC$_{50}$ value: DOTA-3P-RGD$_2$ < DOTA-P-RGD$_2$ < DOTA-P-RGD).

Integrin $\alpha_v\beta_3$ Specificity. Figure 4A compares the 60-min organ uptake of ^{111}In(DOTA-6P-RGD$_4$) in the absence/presence of excess RGD$_2$ (~350 μg/mouse). Co-injection of excess RGD$_2$ significantly blocked the tumor uptake of ^{111}In(DOTA-6P-RGD$_4$) (0.7 %ID/g with RGD$_2$ vs. 11.1 %ID/g without RGD$_2$ at 1 h p.i.). The normal organ uptake of ^{111}In(DOTA-6P-RGD$_4$) was also blocked by the presence of excess RGD$_2$. For example, the uptake of ^{111}In(DOTA-6P-RGD$_4$) in the eyes, heart, intestine, liver, lungs and spleen was 1.4, 0.8, 11.5, 4.0, 3.7 and 2.1 %ID/g, respectively, without excess RGD$_2$, while its uptake values in the same organs were 0.1, 0.4, 0.5, 0.7, 1.2, and 0.5 %ID/g, respectively, with excess RGD$_2$. Similar properties were also observed for other radiolabeled (^{99m}Tc, ^{64}Cu and ^{111}In) cyclic RGD dimers [18, 25, 36-38, 43, 45] and tetramers [20, 31, 46].
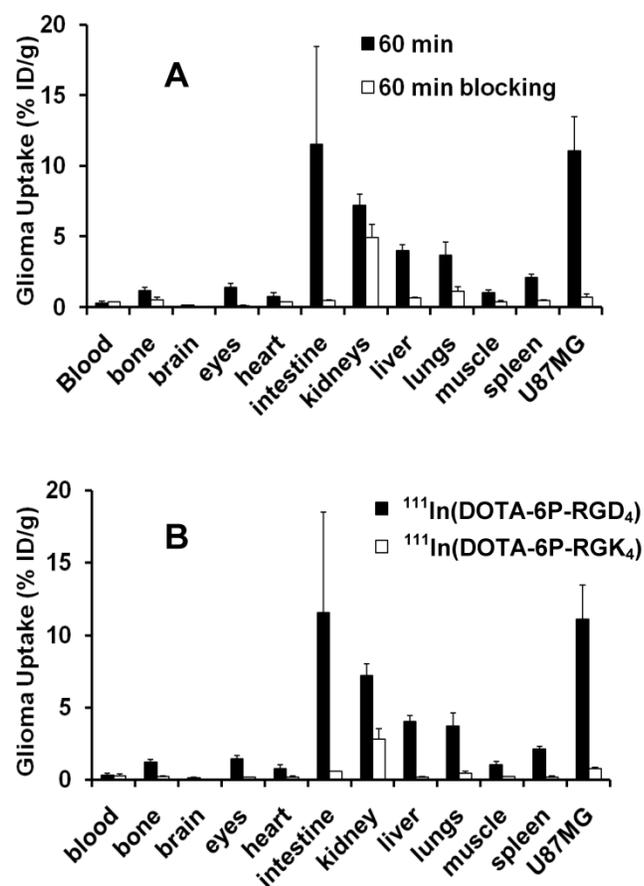
Figure 4. **A**: Comparison of the 60-min biodistribution data of ^{111}In(DOTA-6P-RGD$_4$) in the athymic nude mice (n = 5) bearing U87MG human glioma xenografts in the absence/presence of excess RGD$_2$ to demonstrate its integrin $\alpha_v\beta_3$–specificity. **B**: Comparison of the 60-min biodistribution data of ^{111}In(DOTA-6P-RGD$_4$) and ^{111}In(DOTA-6P-RGK$_4$) in the athymic nude mice (n = 5) bearing U87MG glioma xenografts to demonstrate the RGD-specificity.

RGD Specificity. Figure 4B compares the 60-min uptake of ^{111}In(DOTA-6P-RGD$_4$) and ^{111}In(DOTA-6P-RGK$_4$) in the U87MG glioma and normal organs. As expected, ^{111}In(DOTA-6P-RGK$_4$) had much lower ($p < 0.01$) tumor uptake (0.8 %ID/g) than ^{111}In(DOTA-6P-RGD$_4$) (11.1 %ID/g) due to the low integrin $\alpha_v\beta_3$ binding affinity of DOTA-6P-RGK$_4$. ^{111}In(DOTA-6P-RGK$_4$) also had significantly lower uptake than ^{111}In(DOTA-6P-RGD$_4$) in the normal organs, such as intestine, kidneys, liver, lungs and spleen (Figure 4B). Apparently, replacing c(RGDfK) motifs with c(RGKfD) moieties resulting in a dramatic uptake decrease in the tumor and integrin $\alpha_v\beta_3$–positive organs, particularly intestine, liver, lungs and spleen.

Integrin $\alpha_v\beta_3$ Expression in Normal Organs. To further understand the localization mechanism of ^{111}In radiotracers, the tumor, lung, liver and kidney tissues were harvested, and were then double-stained for the CD31 and integrin β_3 expression. As shown in Figure 5A, U87MG glioma had a high integrin β_3 expression level on both tumor cells and tumor neovasculature. Most of the blood vessels expressing integrin β_3 were seen from the overlay of positive CD31 and β_3 positive staining. Both the liver and lungs had much lower integrin β_3 expression levels than the U87MG tumor. The integrin β_3 expression in kidneys was very low, which seems consistent with the results from blocking experiment (Figure 4A). These results were further confirmed by the Western blot data (Figure 5B).

Imaging Study. Figure 6 illustrates whole-body images of the glioma-bearing mice administered with ^{111}In(DOTA-2P-RGD$_4$), ^{111}In(DOTA-2P4G-RGD$_4$) and ^{111}In(DOTA-6P-RGD$_4$) at 1, 4, 24 and 72 h p.i. The glioma tumors could be clearly visualized with excellent T/B contrast as early as 1 h after injection of ^{111}In(DOTA-2P-RGD$_4$), ^{111}In(DOTA-2P4G-RGD$_4$) and ^{111}In(DOTA-6P-RGD$_4$). All three radiotracers had a long tumor retention time with $t_{1/2} > 30$ h, which was completely consistent with the results obtained from ex-vivo biodistribution studies (Tables 2-4).

Metabolic Stability. Figure 7 shows typical radio-HPLC chromatograms of ^{111}In(DOTA-2P-RGD$_4$) and ^{111}In(DOTA-6P-RGD$_4$) in saline before injection, in urine at 30 min and 120 min p.i., and in feces at 120 min p.i. The radioactivity recovery from the urine and feces samples was >95% in both cases. Attempts to extract radioactivity from the liver and kidneys were not successful due to very limited radioactivity accumulation in both organs. There was little metabolism detected in the urine or feces samples over the 2 h study period for ^{111}In(DOTA-2P-RGD$_4$). ^{111}In(DOTA-2P4G-RGD$_4$) had the same metabolic sta-

bility as ^{111}In(DOTA-2P-RGD$_4$). ^{111}In(DOTA-6P-RGD$_4$) was able to maintain its integrity during its excretion via the renal route. However, there was a significant metabolism during its excretion via the hepatobiliary route. As a matter of fact, only ~45% of ^{111}In(DOTA-6P-RGD$_4$) remained intact in the feces sample. The metabolic instability was also reported for ^{111}In(DOTA-6G-RGD$_4$) [46].
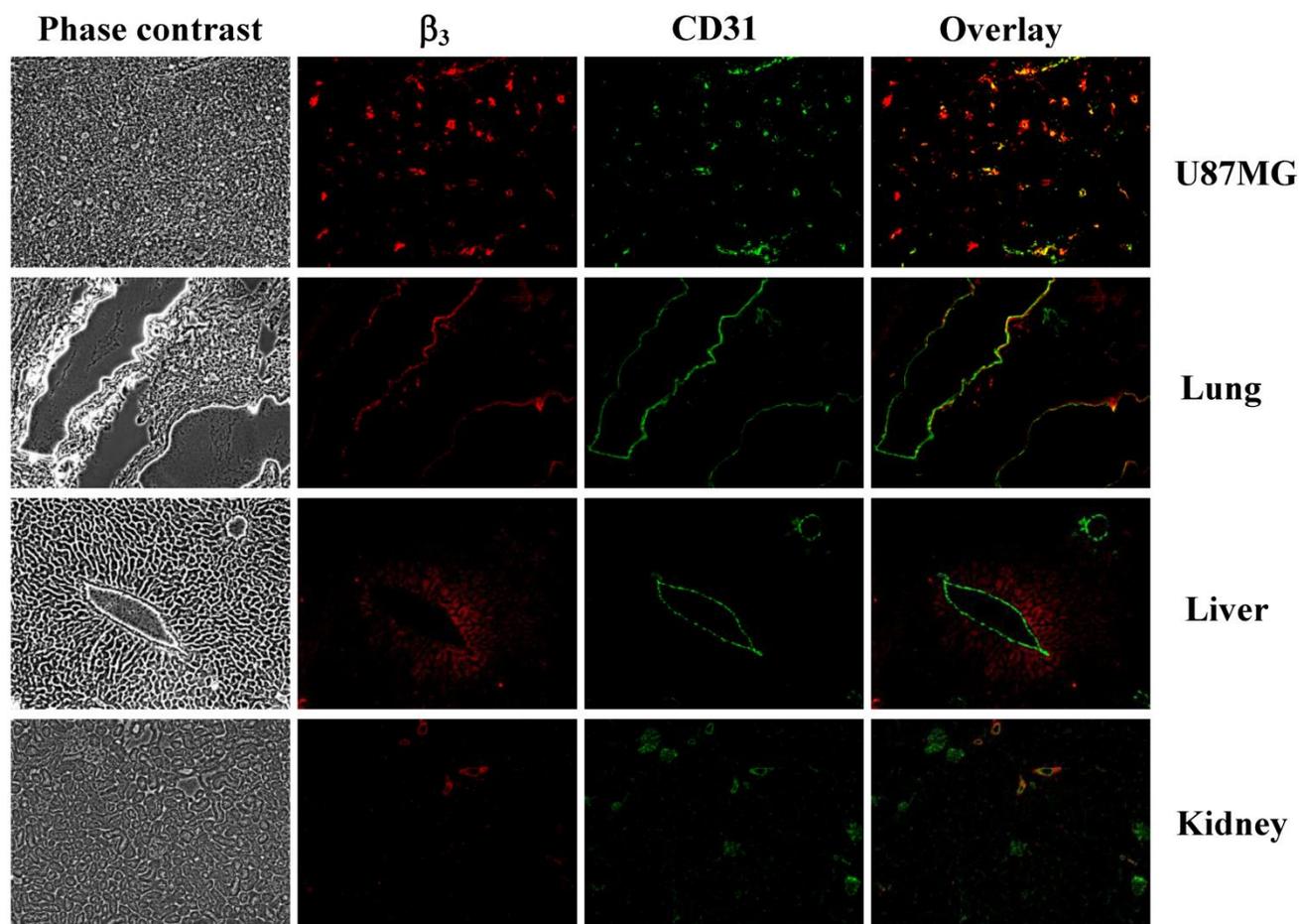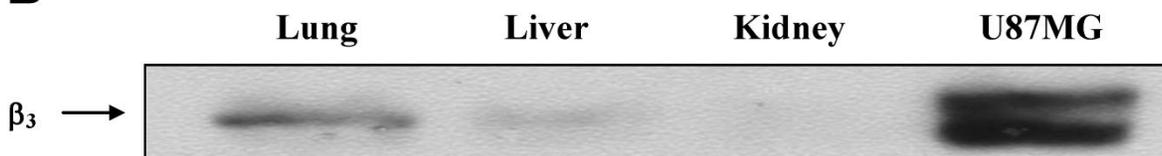

Figure 5. **A**: Representative microscopic fluorescence images of the organ tissues (U87MG glioma, lung, liver and kidney) obtained from the U87MG tumor-bearing mice. For β3 staining (red), frozen tissue slices were incubated with a β3 primary antibody followed by a DyLight 594-conjugated secondary antibody. For CD31 staining (green), slices were incubated with a CD31 primary antibody followed by a FITC-conjugated secondary antibody (×100). Yellow color indicates the overlay of integrin β$_3$ and CD31. Phase contrast pictures were shown as histological reference. **B**: Western blot results showing expression of integrin β$_3$ in U87MG glioma, lungs, liver and kidneys obtained from the U87MG tumor-bearing mice.

^{111}In(DOTA-2P-RGD$_4$)

^{111}In(DOTA-2P4G-RGD$_4$)
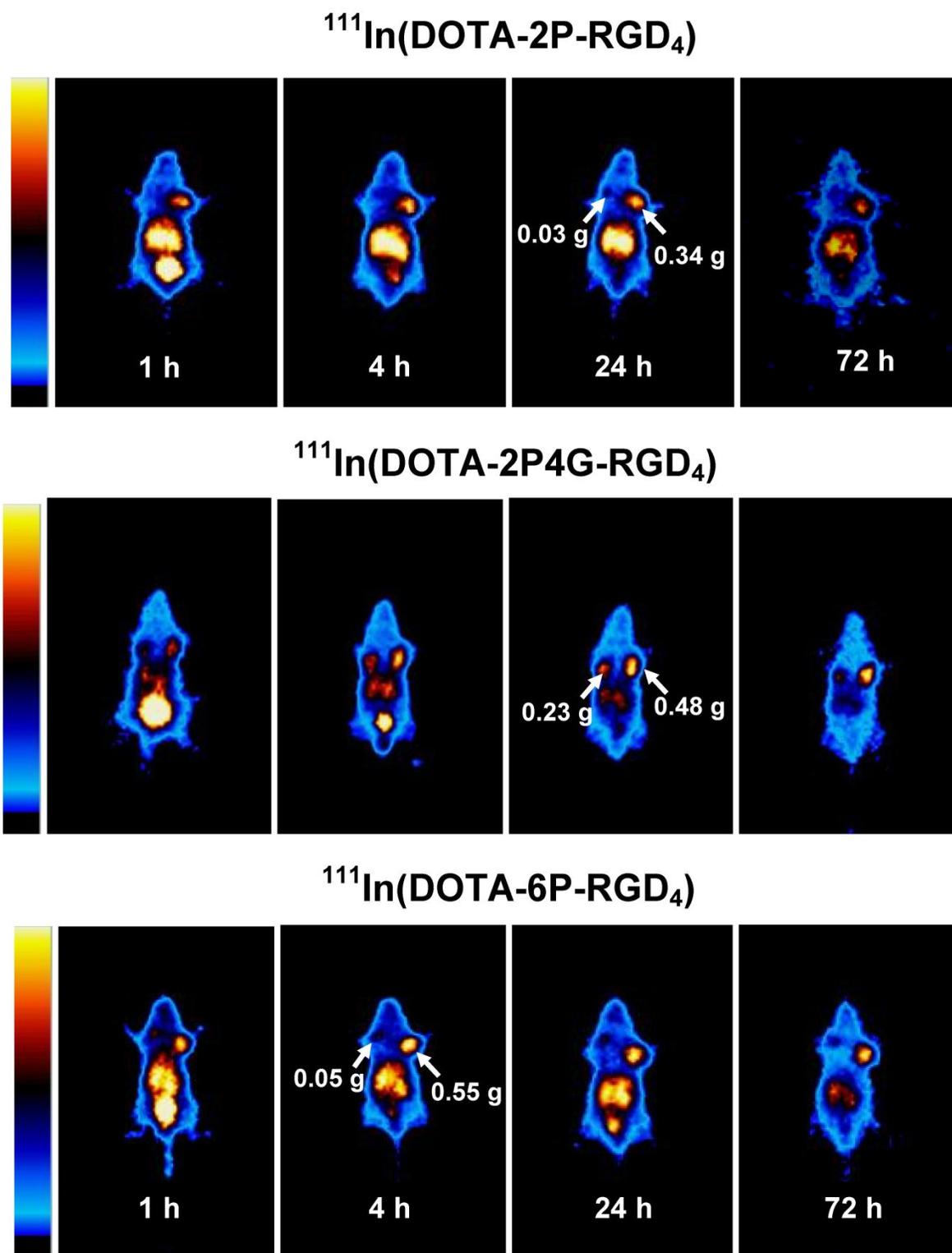
^{111}In(DOTA-6P-RGD$_4$)

Figure 6. The whole-body planar images of the tumor-bearing mice (bearing U87MG human glioma xenografts) administered with ~100 µCi of ^{111}In(DOTA-3P-RGD$_2$) (top), ^{111}In(DOTA-2P-RGD$_4$) (middle) and ^{111}In(DOTA-6P-RGD$_4$) (bottom) to illustrate the long tumor retention times of ^{111}In-labeled cyclic RGD tetramers. Arrows indicate the presence of tumors.
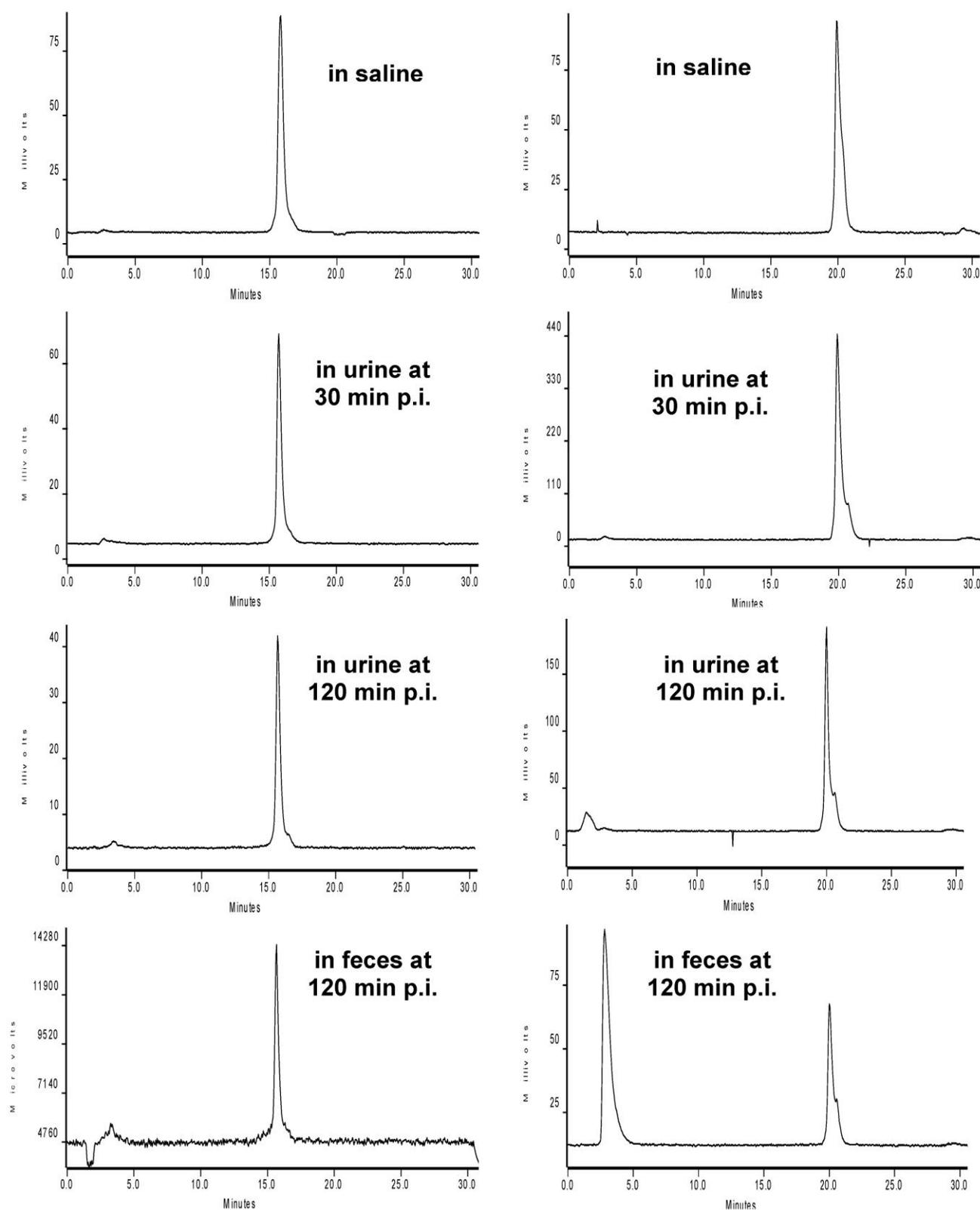
Figure 7. Representative radio-HPLC chromatograms of ^{111}In(DOTA-2P-RGD$_4$) (left) and ^{111}In(DOTA-6P-RGD$_4$) (right) in saline before injection, in urine at 30 min and 120 min p.i., and in feces at 120 min p.i. Each mouse was administered with ~100 μCi radiotracer. ^{111}In(DOTA-2P4G-RGD$_4$) has the same metabolic stability in the same animal model.

Discussion

In this study, we successfully prepared ^{111}In complexes of DOTA-P-RGD, DOTA-P-RGD$_2$, DOTA-2P-RGD$_4$, DOTA-2P4G-RGD$_4$ and DOTA-6P-RGD$_4$. We found that their integrin $\alpha_v\beta_3$ binding affinity follows the order: DOTA-6P-RGD$_4$ ~ DOTA-2P4G-RGD$_4$ ~ DOTA-2P-RGD$_4$ > DOTA-P-RGD$_2$ > DOTA-P-RGD (Figure 2). Previously, we showed that DOTA-3P-RGD$_2$ binds to the integrin $\alpha_v\beta_3$ on U87MG glioma cells in a bivalent fashion due to the increased distance (38 bonds excluding lysine residues) between two cyclic RGD motifs [38, 45]. This study further confirms this observation. For example, the integrin $\alpha_v\beta_3$ binding affinity of DOTA-3P-RGD$_2$ (IC$_{50}$ = 1.5 ± 0.2 nM) is significantly higher (p < 0.01) than that of both DOTA-P-RGD (IC$_{50}$ = 44.3 ± 3.5 nM) and DOTA-P-RGD$_2$ (IC$_{50}$ = 5.0 ± 1.0 nM). The bivalency is further supported by the higher tumor uptake of ^{111}In(DOTA-3P-RGD$_2$) than ^{111}In(DOTA-P-RGD$_2$) and ^{111}In(DOTA-P-RGD) over the 72 h study period (Figure 3).

The integrin $\alpha_v\beta_3$ binding affinities of DOTA-2P-RGD$_4$, DOTA-2P4G-RGD$_4$ and DOTA-6P-RGD$_4$ are only marginally higher than that of DOTA-3P-RGD$_2$ (Figure 2), suggesting that they might share the same bivalency in binding to the integrin $\alpha_v\beta_3$. This conclusion is completely consistent with the similar tumor uptake of ^{111}In(DOTA-3P-RGD$_2$), ^{111}In(DOTA-2P-RGD$_4$), ^{111}In(DOTA-2P4G-RGD$_4$) and ^{111}In(DOTA-6P-RGD$_4$) over the first 24 h (Figure 3). If DOTA-2P-RGD$_4$, DOTA-2P4G-RGD$_4$ and DOTA-6P-RGD$_4$ were tetravalent, they would have had much better integrin $\alpha_v\beta_3$ binding affinity than DOTA-3P-RGD$_2$ while ^{111}In(DOTA-2P-RGD$_4$), ^{111}In(DOTA-2P4G-RGD$_4$) and ^{111}In(DOTA-6P-RGD$_4$) would have had significantly higher initial tumor uptake than that of ^{111}In(DOTA-3P-RGD$_2$).

Two factors (bivalency and the "locally enriched" RGD concentration) contribute to the higher $\alpha_v\beta_3$ binding affinity of multimeric RGD peptides than that of their monomeric counterpart, and the higher tumor uptake of radiolabeled RGD dimers and tetramers than their monomeric analogs [15, 40-46]. The concentration factor exists in all dimers and tetramers. Because of the short distance between two RGD motifs in RGD$_2$, it is unlikely for DOTA-P-RGD$_2$ to be bivalent [15]. However, once the first one is bonded, the "local concentration" of second RGD motif will be dramatically increased in the vicinity of neighboring integrin $\alpha_v\beta_3$ sites. This may explain why DOTA-P-RGD$_2$ has the better integrin $\alpha_v\beta_3$ binding

affinity (Figure 2) than DOTA-P-RGD, and ^{111}In(DOTA-P-RGD$_2$) has higher tumor uptake (Figure 3) than ^{111}In(DOTA-P-RGD). Since IC$_{50}$ values follow the order of DOTA-3P-RGD$_2$ > DOTA-P-RGD$_2$ > DOTA-P-RGD (Figure 2), we believe that both bivalency and concentration factors contribute to the higher tumor uptake of ^{111}In(DOTA-3P-RGD$_2$) than ^{111}In(DOTA-P-RGD) (Figure 3).

DOTA-3P-RGD$_2$ has two cyclic RGD motifs with only one possibility to achieve the bivalency. In DOTA-2P-RGD$_4$, DOTA-2P4G-RGD$_4$ and DOTA-6P-RGD$_4$, however, any two of the four RGD motifs can achieve bivalency due to the longer distance between them. Even though DOTA-2P-RGD$_4$, DOTA-2P4G-RGD$_4$ and DOTA-6P-RGD$_4$ may not be tetravalent, the two extra RGD motifs might contribute to their better integrin $\alpha_v\beta_3$ binding affinity than that of DOTA-3P-RGD$_2$ (Figure 2), and the slightly higher 72-h tumor uptake (Figure 3) for ^{111}In(DOTA-6P-RGD$_4$) than that for ^{111}In(DOTA-3P-RGD$_2$). Higher tumor uptake was also observed for ^{111}In(DOTA-6G-RGD$_4$) than that of ^{111}In(DOTA-3P-RGD$_3$) at 72 h p.i. in the same tumor-bearing animal model [46].

It is very important to note that the ability of a multimeric cyclic RGD peptide to achieve bivalency depends largely on the integrin $\alpha_v\beta_3$ density on tumor cells and tumor neovasculature. If the integrin $\alpha_v\beta_3$ density is high, the distance between two neighboring integrin $\alpha_v\beta_3$ sites will be short, which makes it easier for a multimeric RGD peptide to achieve bivalency. If the integrin $\alpha_v\beta_3$ density is low, the distance between two neighboring integrin $\alpha_v\beta_3$ sites will be long, and it might be more difficult for the same multimeric RGD peptide to achieve simultaneous integrin $\alpha_v\beta_3$ binding. In that situation, the "concentration factor" will be the dominant force contributing to the better integrin $\alpha_v\beta_3$ binding affinity of a multimeric cyclic RGD peptide than that of its monomeric counterpart, and to the higher tumor uptake of the radiolabeled cyclic RGD multimers as compared to their monomeric analogs.

The integrin $\alpha_v\beta_3$-specificity of ^{111}In(DOTA-6P-RGD$_4$) was demonstrated by using RGD$_2$ as the blocking agent. The uptake blockage of ^{111}In(DOTA-6P-RGD$_4$) in the tumor (Figure 4A) suggests that its glioma uptake is indeed mainly integrin $\alpha_v\beta_3$-mediated. The partial blockage of the uptake for ^{111}In(DOTA-6P-RGD$_4$) in eyes, intestine, kidneys, lungs, liver and spleen indicates that the accumulation of ^{111}In(DOTA-6P-RGD$_4$) in these organs is partially integrin $\alpha_v\beta_3$-mediated. This conclusion is supported by the tissue-staining studies (Figure 5A). The low integrin β_3 expression in kidneys (Figure 5B)

suggests that the radiotracer kidney uptake is caused mainly by tubular re-absorption instead of specific integrin $\alpha_v\beta_3$ binding. The RGD-specificity of ^{111}In(DOTA-6P-RGD$_4$) was demonstrated by the extremely low integrin $\alpha_v\beta_3$ binding affinity of DOTA-6P-RGK$_4$ (Figure 2: IC$_{50}$ = 437 ± 35 nM), and the significantly lower tumor uptake (Figure 4B) of ^{111}In(DOTA-6P-RGK$_4$) as compared to that of ^{111}In(DOTA-6P-RGD$_4$). In addition, ^{111}In(DOTA-6P-RGK$_4$) also has low uptake in the intestine, kidneys, liver, lungs and spleen, suggesting that the high uptake of ^{111}In(DOTA-6P-RGD$_4$) in these organs is also RGD-specific.

Non-invasive imaging of integrin $\alpha_v\beta_3$ is highly desirable for patient selection before anti-angiogenic treatment and for more effective monitoring of therapeutic efficacy in the integrin $\alpha_v\beta_3$-positive cancer patients [47-49]. For the tumors to be detectable by SPECT (single photon emission tomography) or PET (positron emission tomography), they must have sufficient accumulation of radioactivity. In this study, we found that small tumors (0.03 – 0.05 g) were clearly visualized (Figure 6) with good contrast in the tumor-bearing mice administered with ^{111}In(DOTA-2P-RGD$_4$), ^{111}In(DOTA-2P4G-RGD$_4$) and ^{111}In(DOTA-6P-RGD$_4$). The tumor detection limit was 3 – 4 mm in diameter using a modified clinical γ-camera. We believe that the tumor detection limit might be < 3 mm using the higher resolution SPECT cameras or SPECT/CT systems with ^{111}In(DOTA-3P-RGD$_2$), ^{111}In(DOTA-2P-RGD$_4$), ^{111}In(DOTA-2P4G-RGD$_4$) and ^{111}In(DOTA-6P-RGD$_4$) as radiotracers. From this view point, all these ^{111}In radiotracers are useful for the early detection of integrin $\alpha_v\beta_3$–positive tumors.

It is well-established that multimerization of cyclic RGD peptides can significantly improve their integrin $\alpha_v\beta_3$-targeting capability [9, 15-41]. However this often leads to more accumulation of the radiolabeled RGD multimers in the integrin $\alpha_v\beta_3$-positive organs, as evidenced by the higher uptake of ^{111}In(DOTA-2P-RGD$_4$) and ^{111}In(DOTA-6P-RGD$_4$) than ^{111}In(DOTA-3P-RGD$_2$) in the intestine, liver and kidneys. As a result, ^{111}In(DOTA-2P-RGD$_4$) and ^{111}In(DOTA-6P-RGD$_4$) have the tumor/liver and tumor/kidney ratios significantly (p < 0.01) lower than those of ^{111}In(DOTA-3P-RGD$_2$) (Figure 3). On the basis of tumor-to-background ratios, we believe that ^{111}In(DOTA-3P-RGD$_2$) is a better diagnostic radiotracer than ^{111}In(DOTA-2P-RGD$_4$) and ^{111}In(DOTA-6P-RGD$_4$). At this moment, we are not clear why ^{111}In(DOTA-2P4G-RGD$_4$) has lower (p < 0.05) intestine uptake than ^{111}In(DOTA-6P-RGD$_4$) and ^{111}In(DOTA-6G-RGD$_4$) (Figure 3) even though they share the same four cyclic RGD motifs. However, it is clear that the G$_3$ and PEG$_4$ linkers between cyclic RGD motifs have a significant impact on biodistribution characteristics of ^{111}In-labeled cyclic RGD tetramers.

For diagnostic radiotracers, the contrast between the targeted organ and surrounding tissues is the first priority. For therapeutic radiotracers, however, maximal delivery of tumoricidal radiation dose becomes critically important. The radiotracer with longer retention time will deliver higher radiation dose to tumors during the same period of time. From this viewpoint, DOTA-6G-RGD$_4$ remains the best for the integrin $\alpha_v\beta_3$-targeted therapeutic ^{90}Y and ^{177}Lu radiotracers since ^{111}In(DOTA-6G-RGD$_4$) has the longest retention time (t$_{1/2}$ ~ 60 h) among four ^{111}In-labeled RGD tetramers (Figure 3). However, one cannot totally ignore its high intestine uptake and low tumor/liver ratios over the 72 h period. Considering the radiotracer uptake in normal organs (particularly intestine and liver), we believe that DOTA-3P-RGD$_2$ and DOTA-2P4G-RGD$_4$ have significant advantages over DOTA-6P-RGD$_4$ and DOTA-6G-RGD$_4$ because the intestine and liver uptake of ^{111}In(DOTA-3P-RGD$_2$) and ^{111}In(DOTA-2P4G-RGD$_4$) is significantly lower than that of ^{111}In(DOTA-6P-RGD$_4$) and ^{111}In(DOTA-6P-RGD$_4$) (Figure 3). It must be noted that there is always a subtle balance between maximizing the radiation dose to tumor cells and minimizing the radiation burden to the surrounding normal tissues or organs.

It is interesting to point out that ^{111}In(DOTA-2P-RGD$_4$) is stable during its renal and hepatobiliary excretion over the 2 h study period (Figure 7). In contrast, ^{111}In(DOTA-6P-RGD$_4$) has a significant metabolism during its hepatobiliary excretion while it remains relatively unchanged during its renal excretion (Figure 7). ^{111}In(DOTA-6G-RGD$_4$) has similar metabolic instability except that only 25% of it remains intact in the feces samples in the same animal model [46]. Although it remains unclear as for what causes this metabolic instability, one thing is clear that the linkers between RGD motifs have a significant impact on the metabolic stability of ^{111}In-labeled cyclic RGD tetramers.

Conclusion

In summary, we evaluated five new radiotracers ^{111}In(L) (L = DOTA-P-RGD, DOTA-P-RGD$_2$, DOTA-2P-RGD$_4$, DOTA-2P4G-RGD$_4$ and DOTA-6P-RGD$_4$) to explore the effect of peptide and PEG$_4$ linker multiplicity on their tumor uptake and T/B ratios. We found that the addition of two PEG$_4$ linkers between two RGD motifs significantly improves the integrin $\alpha_v\beta_3$-targeting capability of cyclic RGD dimers as ev-

idenced by their higher integrin $\alpha_v\beta_3$-binding affinity and the high tumor uptake and better T/B ratios of their radiotracers. We also found that DOTA-2P-RGD$_4$, DOTA-2P4G-RGD$_4$ and DOTA-6P-RGD$_4$ are not tetravalent in binding to integrin $\alpha_v\beta_3$ because increasing the RGD multiplicity from dimers to tetramers didn't significantly improve the radiotracer's initial tumor uptake. However, the extra RGD motifs in DOTA-2P-RGD$_4$, DOTA-2P4G-RGD$_4$ and DOTA-6P-RGD$_4$ might contribute to slightly higher tumor uptake of [111]In(DOTA-2P-RGD$_4$), [111]In(DOTA-2P4G-RGD$_4$) and [111]In(DOTA-6P-RGD$_4$)

than that of [111]In(DOTA-3P-RGD$_2$) at 72 h p.i. Among the ^{111}In-labeled cyclic RGD tetramers evaluated in this animal model, [111]In(DOTA-2P4G-RGD$_4$) has the best tumor/kidney and tumor/liver ratios. The combination of its high tumor uptake, long retention time and low uptake in normal organs suggests that [90]Y(DOTA-2P4G-RGD$_4$) and [177]Lu(DOTA-2P4G-RGD$_4$) may have the potential for radiotherapy of integrin $\alpha_v\beta_3$-positive tumors [50]. Evaluations of their therapeutic efficacy are still in progress, and the result from these studies will be communicated elsewhere.

Abbreviations

c(RGDfK): cyclo(Lys-Arg-Gly-Asp-D-Phe); c(RGDyK): cyclo(Lys-Arg-Gly-Asp-D-Tyr);

E[c(RGDfK)]$_2$ (RGD$_2$): Glu[cyclo(Lys-Arg-Gly-Asp-D-Phe)-cyclo(Lys-Arg-Gly-Asp-D-Phe)];

DOTA: 1,4,7,10-tetraazacyclododecane-1,4,7,10-tetracetic acid;

PEG$_4$: 15 amino-4,710,13-tetraoxapentadecanoic acid;

PEG$_4$-E[G$_3$-c(RGDfK)]$_2$: PEG$_4$-Glu{cyclo[Lys(Gly-Gly-Gly)-Arg-Gly-Asp-D-Phe]}-cyclo[Lys(Gly-Gly-Gly)-Arg-Gly-Asp-D-Phe]};

PEG$_4$-E[PEG$_4$-c(RGDfK)]$_2$: PEG$_4$-Glu{cyclo[Lys(PEG$_4$)-Arg-Gly-Asp-D-Phe]-cyclo[Lys(PEG$_4$)-Arg-Gly-Asp-D-Phe]};

PEG$_4$-E[PEG$_4$-c(RGKfD)]$_2$: PEG$_4$-Glu{cyclo[Arg-Gly-Lys(PEG$_4$)-D-Phe-Asp]-cyclo[Arg-Gly-Lys(PEG$_4$)-D-Phe-Asp]};

E{E[c(RGDfK)]$_2$}$_2$ (RGD$_4$): Glu{Glu[cyclo(Lys-Arg-Gly-Asp-D-Phe)]-cyclo(Lys-Arg-Gly-Asp-D-Phe)}-{Glu[cyclo(Lys-Arg-Gly-Asp-D-Phe)]-cyclo(Lys-Arg-Gly-Asp-D-Phe)};

E{PEG$_4$-E[c(RGDfK)]$_2$}$_2$: Glu{PEG$_4$-Glu[cyclo(Lys-Arg-Gly-Asp-D-Phe)]-cyclo(Lys-Arg-Gly-Asp-D-Phe)}-{PEG$_4$-Glu[cyclo(Lys-Arg-Gly-Asp-D-Phe)]-cyclo(Lys-Arg-Gly-Asp-D-Phe)};

E{PEG$_4$-E[G$_3$-c(RGDfK)]$_2$}$_2$: Glu{PEG$_4$-Glu[cyclo(Lys(Gly-Gly-Gly)-Arg-Gly-Asp-D-Phe)]-cyclo(Lys(Gly-Gly-Gly)-Arg-Gly-Asp-D-Phe)}-{PEG$_4$-Glu[cyclo(Lys(Gly-Gly-Gly)-Arg-Gly-Asp-D-Phe)]-cyclo(Lys(Gly-Gly-Gly)-Arg-Gly-Asp-D-Phe)};

E{PEG$_4$-E[PEG$_4$-c(RGDfK)]$_2$}$_2$: Glu{PEG$_4$-Glu[cyclo(Lys(PEG$_4$)-Arg-Gly-Asp-D-Phe)]-cyclo(Lys(PEG$_4$)-Arg-Gly-Asp-D-Phe)}-{PEG$_4$-Glu[cyclo(Lys(PEG$_4$)-Arg-Gly-Asp-D-Phe)]-cyclo(Lys(PEG$_4$)-Arg-Gly-Asp-D-Phe)};

E{PEG$_4$-E[PEG$_4$-c(RGKfD)]$_2$}$_2$: Glu{PEG$_4$-Glu[cyclo(Arg-Gly-Lys(PEG$_4$)-D-Phe-Asp)]-cyclo(Arg-Gly-Lys(PEG$_4$)-D-Phe-Asp)}-{PEG$_4$-Glu[cyclo(Arg-Gly-Lys(PEG$_4$)-D-Phe-Asp)]-cyclo(Arg-Gly-Lys(PEG$_4$)-D-Phe-Asp)}.

Acknowledgement

Conflict of Interest

The authors have declared that no conflict of interest exists.

References

1. Weber WA, Haubner R, Vabuliene E, et al. Tumor angiogenesis targeting using imaging agents. Q J Nucl Med. 2001; 45: 179-82.
2. Liu S, Edwards DS. Fundamentals of receptor-based diagnostic metalloradiopharmaceuticals. Top Curr Chem. 2002; 222: 259-78.
3. Van de Wiele C, Oltenfreiter R, De Winter O, et al. Tumor angiogenesis pathways: related clinical issues and implications for nuclear medicine imaging. Eur J Nucl Med. 2002; 29: 699-709.
4. Liu S, Robinson SP, Edwards DS. Integrin $\alpha_v\beta_3$ directed radiopharmaceuticals for tumor imaging. Drugs Fut. 2003; 28: 551-64.
5. Haubner R, Wester HJ. Radiolabeled tracers for imaging of tumor angiogenesis and evaluation of anti-angiogenic therapies. Curr Pharm Des. 2004; 10: 1439-55.
6. Liu S, Robinson SP, Edwards DS. Radiolabeled integrin $\alpha_v\beta_3$ antagonists as radiopharmaceuticals for tumor radiotherapy. Top Curr Chem. 2005; 252: 193-216.
7. Chen X. Multimodality imaging of tumor integrin $\alpha_v\beta_3$ expression. Mini-Rev Med Chem. 2006; 6: 227-34.
8. Meyer A, Auernheimer J, Modlinger A, et al. Targeting RGD recognizing integrins: drug development, biomaterial research, tumor imaging and targeting. Curr Pharm Des. 2006; 12: 2723-47.
9. Liu S. Radiolabeled multimeric cyclic RGD peptides as integrin $\alpha_v\beta_3$-targeted radiotracers for tumor imaging. Mol. Pharm. 2006; 3: 472-87.

10. Cai W, Chen X. Multimodality molecular imaging of tumor angiogenesis. J Nucl Med. 2008; 49 (Suppl 2): 113S-128S.

11. Haubner R, Wester HJ, Senekowitsch-Schmidtke R, et al. RGD-peptides for tumor targeting: biological evaluation of radioiodinated analogs and introduction of a novel glycosylated peptide with improved biokinetics. J Lab Compd Radiopharm. 1997; 40: 383-5.

12. Haubner R, Bruchertseifer F, Bock M, et al. Synthesis and biological evaluation of ^{99m}Tc-labeled cyclic RGD peptide for imaging integrin $\alpha_v\beta_3$ expression. Nuklearmedizin. 2004; 43: 26-32.

13. Haubner R, Wester HJ, Reuning U, et al. Radiolabeled $\alpha_v\beta_3$ integrin antagonists: a new class of tracers for tumor imaging. J Nucl Med. 1999; 40: 1061-71.

14. Haubner R, Wester HJ, Weber WA, et al. Noninvasive imaging of $\alpha_v\beta_3$ integrin expression using ^{18}F-labeled RGD-containing glycopeptide and positron emission tomography. Cancer Res. 2001; 61: 1781-5.

15. Liu S. Radiolabeled cyclic RGD peptides as integrin $\alpha_v\beta_3$-targeted radiotracers: maximizing binding affinity via bivalency. Bioconj Chem. 2009; 20: 2199-213.

16. Thumshirn G, Hersel U, Goodman SL, et al. Multimeric cyclic RGD peptides as potential tools for tumor targeting: solid-phase peptide synthesis and chemoselective oxime ligation. Chem Eur J. 2003; 9: 2717-25.

17. Poethko T, Schottelius M, Thumshirn G, et al. Chemoselective pre-conjugate radiohalogenation of unprotected mono- and multimeric peptides via oxime formation. Radiochimica Acta. 2004; 92: 317-27.

18. Chen X, Liu S, Hou Y, et al. MicroPET imaging of breast cancer α_v-integrin expression with ^{64}Cu-labeled dimeric RGD peptides. Mol. Imaging Biol. 2004; 6: 350-9.

19. Chen X, Tohme M, Park R, et al. MicroPET imaging of breast cancer α_v-integrin expression with ^{18}F-labeled dimeric RGD peptide. Mol. Imaging 2004; 3: 96-104.

20. Wu Y, Zhang X, Xiong Z, et al. MicroPET imaging of glioma integrin $\alpha_v\beta_3$ expression using ^{64}Cu-labeled tetrameric RGD peptide. J Nucl Med. 2005; 46: 1707-18.

21. Zhang X, Xiong Z, Wu Y, et al. Quantitative PET imaging of tumor integrin $\alpha_v\beta_3$ expression with ^{18}F-FRGD$_2$. J Nucl Med. 2006; 47: 113-21.

22. Wu Z, Li Z, Chen K, et al. Micro-PET of tumor integrin $\alpha_v\beta_3$ expression using ^{18}F-labeled PEGylated tetrameric RGD peptide (^{18}F-FPRGD4). J Nucl Med. 2007; 48: 1536-44.

23. Liu S, Edwards DS, Ziegler MC, et al. ^{99m}Tc-labeling of a hydrazinonictotinamide-conjugated vitronectin receptor antagonist useful for imaging tumor. Bioconj Chem. 2001; 12: 624-9.

24. Liu S, Hsieh WY, Kim YS, et al. Effect of coligands on biodistribution characteristics of ternary ligand ^{99m}Tc complexes of a HYNIC-conjugated cyclic RGDfK dimer. Bioconj Chem. 2005; 16: 1580-8.

25. Jia B, Shi J, Yang Z, et al. ^{99m}Tc-labeled cyclic RGDfK dimer: initial evaluation for SPECT imaging of glioma integrin $\alpha_v\beta_3$ expression. Bioconj Chem. 2006; 17: 1069-76.

26. Liu S, He ZJ, Hsieh WY, et al. Impact of PKM linkers on biodistribution characteristics of the ^{99m}Tc-labeled cyclic RGDfK dimer. Bioconj Chem. 2006; 17: 1499-507.

27. Janssen ML, Oyen WJG, Dijkgraaf I, et al. Tumor targeting with radiolabeled $\alpha_v\beta_3$ integrin binding peptides in a nude mouse model. Cancer Res. 2002; 62: 6146-51.

28. Janssen M, Oyen WJG, Massuger LFAG, et al. Comparison of a monomeric and dimeric radiolabeled RGD-peptide for tumor targeting. Cancer Biother Radiopharm. 2002; 17: 641-6.

29. Dijkgraaf I, Kruijtzer JAW, Liu S, et al. Improved targeting of the $\alpha_v\beta_3$ integrin by multimerization of RGD peptides. Eur J Nucl Med Mol Imaging. 2007; 34: 267-73.

30. Dijkgraaf I, Liu S, Kruijtzer JAW, et al. Effect of linker variation on the in vitro and in vivo characteristics of an ^{111}In-labeled RGD Peptide. Nucl Med Biol. 2007; 34: 29-35.

31. Liu S, Hsieh WY, Jiang Y, et al. Evaluation of a ^{99m}Tc-labeled cyclic RGD tetramer for non-invasive imaging integrin $\alpha_v\beta_3$-positive breast cancer. Bioconj Chem. 2007; 18: 438-46.

32. Liu S, Kim YS, Hsieh WY, et al. Coligand effects on solution stability, biodistribution and metabolism of ^{99m}Tc-labeled cyclic RGDfK tetramer. Nucl Med Biol. 2008; 35: 111-21.

33. Jia B, Liu Z, Shi J, et al. Linker effects on biological properties of ^{111}In-labeled DTPA conjugates of a cyclic RGDfK dimer. Bioconj Chem. 2008; 19: 201-10.

34. Wang JJ, Kim YS, He ZJ, et al. ^{99m}Tc-labeling of HYNIC-conjugated cyclic RGDfK dimer and tetramer using EDDA as coligand. Bioconj Chem. 2008; 19: 634-42.

35. Li ZB, Chen K, Chen X. ^{68}Ga-labeled multimeric RGD peptides for microPET imaging of integrin $\alpha_v\beta_3$ expression. Eur J Nucl Med Mol Imaging. 2008; 35: 1100-8.

36. Wang L, Shi J, Kim YS, et al. Improving tumor-targeting capability and pharmacokinetics of ^{99m}Tc-labeled cyclic RGD dimers with PEG$_4$ linkers. Mol Pharm. 2009; 6: 231-45.

37. Shi J, Wang L, Kim YS, et al. Improving tumor uptake and excretion kinetics of ^{99m}Tc-labeled cyclic Arginine-Glycine-Aspartic (RGD) dimers with triglycine linkers. J Med Chem. 2008; 51: 7980-90.

38. Shi J, Kim YS, Zhai S, et al. Improving tumor uptake and pharmacokinetics of ^{64}Cu-labeled cyclic RGD peptide dimers with Gly$_3$ and PEG$_4$ Linkers. Bioconj. Chem. 2009; 20: 750-9.

39. Liu Z, Liu S, Wang F, et al. Non-invasive imaging of tumor integrin expression using ^{18}F-labeled RGD dimer peptide with PEG$_4$ linkers. Eur J Nucl Med Mol Imaging. 2009; 36: 1296-307.

40. Shi J, Kim YS, Chakraborty S, et al. 2-Mercaptoacetylglycylglycyl (MAG$_2$) as a bifunctional chelator for ^{99m}Tc-labeling of cyclic RGD dimers: effects of technetium chelate on tumor uptake and pharmacokinetics. Bioconj Chem. 2009; 20: 1559-68.

41. Shi J, Wang L, Kim YS, et al. ^{99m}TcO(MAG$_2$-3G$_3$-dimer): a new integrin $\alpha_v\beta_3$-targeted SPECT radiotracer with high tumor uptake and favorable pharmacokinetics. Eur J Nucl Med Mol Imaging. 2009; 36: 1874-84.

42. Liu Z, Niu G, Shi J, et al. ^{68}Ga-labeled cyclic RGD dimers with Gly$_3$ and PEG$_4$ linkers: promising agents for tumor integrin $\alpha_v\beta_3$ PET imaging. Eur J Nucl Med Mol Imaging. 2009; 36: 947-57.

43. Liu Z, Jia B, Shi J, et al. Tumor uptake of the RGD dimeric probe ^{99m}Tc-G$_3$-2P$_4$-RGD$_2$ is correlated with integrin $\alpha_v\beta_3$ expressed on both tumor cells and neovasculature. Bioconj Chem. 2010; 21: 548-55.

44. Dijkgraaf I, Yim CB, Franssen GM, et al. PET imaging of $\alpha_v\beta_3$ integrin expression in tumours with ^{68}Ga-labeled mono-, di- and tetrameric RGD peptides. Eur J Nucl Med Mol Imaging. 2011; 38: 128-37.

45. Shi J, Kim YS, Chakraborty S, et al. Impact of bifunctional chelators on biological properties of ^{111}In-labeled cyclic peptide RGD dimers. Amino Acids 2010; [Epub ahead of print].

46. Chakraborty S, Shi J, Kim YS, et al. Evaluation of ^{111}In-labeled cyclic RGD peptides: tetrameric not tetravalent. Bioconj Chem. 2010; 21: 969-78.

47. Cai W, Rao J, Gambhir SS, et al. How molecular imaging is speeding up antiangiogenic drug development? Mol Cancer Ther. 2006; 5: 2624-33.

48. Niu G, Chen X. Has molecular and cellular imaging enhanced drug discovery and drug development? Drugs R D. 2008; 9: 351-68.

49. Cai W, Niu G, Chen X. Imaging of integrins as biomarkers for tumor angiogenesis. Curr Pharm Des. 2008; 14: 2943-73.

50. Liu Z, Wang F, Chen X. Integrin targeted delivery of radiotherapeutics. Theranostics. 2011; 1: 201-10.